æ

16. CYTOSKELETON, CELL SHAPE, AND MOTILITY

4 September 2021

As in multicellular organisms, single cells are confronted with challenges associated with structural support and delivery of bioproducts, albeit at a different scale. Most cells rely on endoskeletons (filaments and tubules) and/or exoskeletons (cell walls) to maintain cell-shape integrity. Cell division requires membrane-deforming proteins, and in eukaryotes, various modes of internal cellular movement require cytoskeletons for the transport of large cargoes, such as vesicles. Central to all of these cellular features are protein fibrils and sheets comprised of long concatenations of monomeric subunits. In eukaryotes, long, linear fibers serve as highways for the walking movement of special cargo-carrying molecular motors fueled by ATP hydrolysis.

This chapter continues an exploration of the internal anatomy and natural history of cellular components, exploring the evolutionary diversification of cytoskeletal proteins and their varied functions, as well as the expansion of diverse sets of eukaryote-specific molecular motors and their roles in intracellular transport. Although prokaryotes are often viewed as being devoid of such proteins, fibrillar proteins in prokaryotes have comparable diversity to that in eukaryotes, playing central but contrasting roles in structural support and cell division. How fundamental features such as cell division were carried out prior to the origin of filament-forming proteins is unknown, but the emergence of self-assembling fibrils would have been a watershed moment for evolution, providing new opportunities for cellular features requiring structural support systems.

In eukaryotes, fibrillar proteins are also central to swimming with flagella and crawling with pseudopodia, so this chapter will explore a few generalities with respect to cellular motion. The limits to motility of single-celled organisms will be shown to follow some general scaling laws across the Tree of Life. Prokaryotes and eukaryotes both use flagella to swim, and such structures are sometimes suggested to be so complex as to defy an origin by normal evolutionary processes. However, not only are there plausible routes for the emergence of flagella via modifications of pre-existing cellular features, but prokaryotic and eukaryotic flagella evolved independently and operate in completely different manners.

The Basic Cytoskeletal Infrastructure

The three major groups of fibrillar proteins distributed across the Tree of Life will be discussed in the following sections. The most celebrated members, actins and tubulins, are often viewed as eukaryotic innovations, However, relatives of both families have diverse functions in various prokaryotic lineages, e.g., cell-shape sculpting, cell division, plasmid replication partitioning, and magnetosomes (Ozyamak et al. 2013). This phylogenetic distribution suggests that the antecedents of most of the major fibril-forming proteins were present as early as LUCA. Moreover, it bears noting that additonal types of filament-forming proteins, not discussed below, are sequestered in various prokaryotic lineages (Wagstaff and Löwe 2018). This supports the idea that fibrils are not particularly difficult to evolve, the main requirements being the emergence of a heterologous interface for fibril formation and a presumed selective advantage (Chapter 13). Indeed, as noted in Chapter 13, a major challenge in the evolution of many proteins may be the avoidance of producing open chains.

All filaments are comprised of chains of noncovalently linked monomeric subunits. Nonetheless, despite sequence divergence at the level of monomers, fibrillar proteins from very distant species faithfully assemble and function in novel host species (Horio and Oakley 1994; Osawa and Erickson 2006). General reviews can be found in Wickstead and Gull (2011), Erickson (2007), Michie and Löwe (2006), and Löwe and Amos (2008). An overview of the energetic costs of producing cytoskeletal proteins in eukaryotes is provided in Foundations 16.1.

Actins. Comprised of one of the most abundant proteins within eukaryotic cells, actin polymers play diverse roles, including cell-cortex formation, vesicle trafficking, cell division, endocytosis, and amoeboid movement. Actin filaments are homopolymeric, double-stranded, and helical, typically 5 to 9 nm in diameter (Figure 16.1). Free actin monomers are generally bound to ATP, and upon joining a filament undergo ATP hydrolysis. Actin filaments are polar, with the monomeric subunits being added at the plus (barbed) end. Combined with removal at the minus end, this can result in the "apparent" movement of a filament in a treadmilling-like process (Carlier and Shekhar 2017) – at a critical concentration of monomers, the end-specific rates of addition and removal become equal, with no net filament growth and simple movement of the ends.

Multiple families commonly exist within a species, with different copies often being assigned to different intracellular functions (e.g., Sehring et al. 2007; Joseph et al. 2008; Velle and Fritz-Laylin 2019), although yeasts and *Giardia* encode only a single copy. Numerous additional families of proteins are associated with the assembly of actin cables and networks. For example, at least eight families of actin-related proteins (ARPs), related to actins by gene duplication, are involved in the nucleation of new filaments and patterning of branches off parental actins (Goodson and Hawse 2002). Profilins are involved in the regulated delivery of monomers to growing filaments, a process that is further facilitated by formins. WASP (Wiscott-Aldrich syndrome protein)-family proteins are involved in context-specific catalysis of ARP-induced branch growth, and appear to be essential in crawling motility (Fritz-Laylin et al. 2017). At least three major families of such proteins are inferred to have been present in LECA, and these have in turn diversified enormously among phylogenetic lineages, while also being lost from some lineages in coordination with ARP loss (Veltman and Insall 2010; Kollmar et al. 2012).

Actin-like proteins in bacteria share the basic structural architecture of eukaryotic actin (including the contact sites at monomer interfaces and the ATP binding site involved in polymerization/depolymerization). Although this suggests likely phylogenetic relatedness (Ghoshdastider et al. 2015), they are substantially different sequence-wise (sometimes to the point of not being identifiable by this means; Bork et al. 1992). The bacterial actin relatives also have diverse functions, but are sporadically distributed over the bacterial phylogeny, usually with only one or two types per species. For example, MreB is involved in the maintenance of rod-shaped cells, forming helical shapes around the cell periphery (Margolin 2009). ParR acts like a centromeric-binding protein, elongating and pushing plasmid copies to the opposite ends of the dividing parental cell with an actin-like concatamer of ParM (Salje et al. 2010). In some bacteria, magnetite crystals organize along a MamK filament, creating a magnet used in orientation (Bazylinski and Frankel 2004). Expression of DivB in foci during times of stress induces *Streptomyces* to grow into branching, filamentous mats.

Although usually consisting of double-stranded helices, these broad families of bacterial filaments vary widely with respect to the periodicity of twists, the degree of staggering between strands, and even the direction of helix winding (handedness). A protein harbored by the archaebacterium *Pyrobaculum calidifontis,* crenactin, has closer sequence similarity to eukaryotic actins and again shares similar helical structure (Ettema et al. 2011; Braun et al. 2015; Izoré et al. 2016). All of these observations strongly suggest that an actin-like protein was present in LUCA.

Tubulins. The second major types of eukaryotic fibrils are comprised of tubulin monomers, which initially assemble into thin protofilaments through the stepwise addition of heterodimers of α- and β-tubulin subunits. Ultimately, 13 protofilaments are typically assembled into hollow cylindrical microtubules, approximately 25 nm in diameter (Figure 16.1). Unlike actins, which use ATP hydrolysis in assembly, tubulins use GTP hydrolysis. The minus ends of microtubules are generally anchored at a microtubule-organizing center, such as a centrosome, a spindle-pole body, or a basal body. Growth and contraction occurs at the opposite end in a process known as dynamic instability, which plays a central role in various aspects of cell motility (Gardner et al. 2013; Akhmanova and Steinmetz 2015).

As with actins, there is clear evidence that the antecedents of tubulins were present in LUCA, the most telling of which is FtsZ, a bacterial protein that assembles into homomeric filaments that can form bundles (but not organized microtubules). FtsZ monomeric subunits are nearly identical in structure to tubulin monomers, and despite having very low sequence identity, the few sites conserved between FtsZ and tubulin are almost all involved in GTP binding (Löwe and Amos 2009). FtsZ produces contractile rings that guide bacterial cell division, although at least one bacterial group (the planctomycetes) deploys an unrelated protein for such purposes (Van Niftrik et al. 2009). Notably, FtsZ-related proteins are also present in numerous eukaryotes, where they form the division ring responsible for fission of mitochondria and chloroplasts (presumably a vestige of these organelles having arising by bacterial endosymbiosis; Chapter 23). Such proteins have, however, been lost from a number of eukaryotic lineages (including metazoans), implying alternative modes of organelle division (Kiefel et al. 2004; Bernander and Ettema 2010).

α- and β-tubulin are products of an ancient gene duplication that preceded LECA. Moreover, in addition to the α and β families, at least six other distinct tubulin families are known in eukaryotes (although only γ seems to be present in all lineages), and these are generally deployed in different cellular contexts, e.g., basal bodies out of which cilia and flagella grow, rails for vesicle transport, and mitotic/meiotic spindles used for chromosome separation.

Such diversification of function, sometimes called the multi-tubulin hypothesis (McKean et al. 2001; Dutcher 2003), extends to different variants within the α and β subtypes. Consider, for example, two closely related amoeboid protists, with extreme forms of pseudopodia. Foraminiferans produce branching networks (reticulopodia) that assist in prey capture, whereas radiolarians produce stiff, spine-like axopodia that assist in floating and capturing prey. Each group deploys a uniquely modified β tubulin to construct the helical filaments involved in such structures (Hou et al. 2013).

Tubulins can also be assembled into higher-order structures. For example, most eukaryotes harbor a pair of barrel-shaped organelles called centrioles, comprised largely of microtubules. With few exceptions, centrioles consist of rings of nine microtubule triplets, with the overall structure resembling a cartwheel. Throughout eukaryotes, centrioles serve as the basal body from which flagella and cilia grow (below). Phylogenetic analysis implies their presence in the ancestral eukaryote, with losses in a few lineages, including yeasts and land plants (Carvalho-Santos et al. 2010, 2011; Hodges et al. 2010).

In animals and some fungi, centrioles play a second role, comprising the centrosome that serves as the organizing center from which the mitotic spindle expands during cell division (Chapter 10). Some insects have evolved centrioles with much more elaborate structures than the conventional nine-triplet cartwheel, and a few protists have simpler structures (Gönczy 2012), although the mechanisms driving such change remain unknown. During sexual reproduction in animals, the centriole is excluded from the egg and introduced via the sperm, possibly an evolutionary outcome of sexual conflict and/or sperm competition and causally related to the high rate of evolution of centriolar protein sequences (Carvalho-Santos et al. 2011; Ross and Normark 2015).

Although the 13-protofilament microtubule appears to be unique to eukaryotes, related structures exist in some prokaryotes. For example, some members of the Verrucomicrobiales genus *Prosthecobacter* contain two tubulin-like genes, BtubA and BtubB, that form heterodimers, which in turn polymerize into four-filament microtubules capable of dynamic instability and are also joined by a third protein seemingly related to a eukaryotic motor protein (Pilhofer et al. 2011; Deng et al. 2017). Acquisition of such proteins by ancient horizontal transfer from a eukaryote cannot be ruled out, but regardless, the altered assembly clearly indicates the potential for variation in microtubule structure. The general picture is that FtsZ and the tubulins are all members of a common family of proteins, with BtubA/B having evolved a heterodimeric form after gene duplication.

One of the more interesting aspects of actin and tubulin-related proteins is that they have seemingly exchanged roles in cell division in eukaryotes vs. prokaryotes. As noted above, cytokinesis involves a tubulin-like ring (FtsZ) in bacteria but an actin ring in eukaryotes. In contrast, whereas microtubules are universally used

to move chromosomes apart in eukaryotes, actin-like molecules are involved in the partitioning of plasmid genomes in most bacteria (Larsen et al. 2007; Salje et al. 2010; Szewczak-Harris and Löwe 2018), although tubulin-like molecules are used in still others (Larsen et al. 2007). This differential utilization of fibrillar proteins provides a clear example of convergent evolution of the same function from substantially different starting points. Notably, phylogenetic subgroups of the archaea also appear to deploy diverse sets of filaments in cytokinesis, some FtsZ-like and others actin-like, including a protein involved in the partitioning of endosomes in eukaryotes (Lindås et al. 2008; Samson and Bell 2009; Makarova et al. 2010; Pelve et al. 2011).

Finally, as will be noted below, actins and tubulins act in consortia with motor proteins to accomplish a wide array of intracellular functions. However, these fibrils are also capable of work on their own, creating pushing forces that can be used to move various organelles and to deform the cell membrane. How can this occur if the fibrils grow at the tips that are in contact their targets? Although not all of the details are worked out, it appears that continued fibril elongation occurs by a sort of Brownian motion ratchet. Slight fluctuations at points of contact allow occasional room for a new monomer to join the pushing end of the fibril, thereby ratcheting the point of contact forward.

Intermediate filaments. A third group of fibril forming proteins known as intermediate filaments are quite unlike tubulins and actins structurally, forming unpolarized cables and sheets that are not dynamic. Although such structures are ultimately assembled from dimeric subunits, unlike the situation in actins and tubulins, these organize into coiled coils before further development into higher-order structures (Figure 16.1). Intermediate filaments are mostly confined to metazoans and slime molds, where they have a variety of functions involved in structural support, e.g., lamins, keratins, and desmins (Preisner et al. 2018). This restricted distribution, sequestered to one clade, suggests a post-LECA origin. However, a potential homolog, crescentin, exists in the bacterium *Caulobacter crescentus* and is thought to determine cell shape.

Cell Shape

Cells come in a wide variety of sizes and shapes. Indeed, unicellular eukaryotes often have such characteristic shapes that they can sometimes be used as diagnostics for species identification, e.g., as in diatoms and dinoflagellates. Bacteria also have a wide range of possible cell shapes (Young 2006), although only a small number of these are commonly utilized. Most bacteria are either spherical or rod-shaped, having an average axial (length:width) ratio of ~ 3, with nonmotile cells being spheres more frequently than are flagellated cells (Dusenbery 1998; Young 2006). When confined to constricted settings or forced to bend, bacteria can take on a wide variety of shapes, but upon release to more natural settings, they return to their characteristic shapes (Männik et al. 2009; Amir et al. 2014), demonstrating both a capacity for plasticity and a significant degree of genetic determinism.

Cytoskeletal fibrils and cell walls provide support structures essential for main-

taining shape, although the precise molecular mechanisms governing the diversification of cell shape remain largely unknown. The evolutionary advantages of alternative cell shapes are also unknown in most cases, although a variety of hypothetical scenarios can be envisioned (Pirie 1973; Marshall 2011; Pančić et al. 2019). For example, given the known behavior of different shapes within fluids, the relative advantages of alternative forms, e.g., spheres, oblate spheroids (flat ellipsoids), and prolate spheroids (elongate ellipsoids, close to rods in form), can be determined from a purely biophysical perspective (Dusenbery 1998). Under this view, if there were to be a premium on increased surface area (as would be the case if cell surface area limits its nutrient uptake), disk-shaped cells would be expected to be common. However, these are almost never found among bacteria (one exception being *Haloquadratum,* which forms flat squares), although some diatoms have such forms. Spheres (which have a minimum surface:volume ratio) have the highest rate of diffusion through a liquid, and would be selectively promoted if random dispersal were to be advantageous. However, the sedimentation rate of spheres also exceeds that of all other ellipsoids, which may be disadvantageous under many conditions, e.g., phytoplankton sinking out of the photic zone. Up to a 2.4× reduction in sinking rate occurs with a rod-like form, but this maximum effect requires an axial ratio of ~ 30, far beyond what is typically observed (some needle-shaped diatoms being an exception). Owing to reduced drag, swimming efficiency is greatest for a rod with an axial ratio of 2, but this is smaller than what is typically seen.

Why then are rod-shaped bacteria so common? Rods generally grow only in length (not width), essentially keeping the surface area:volume constant over the cell cycle (as the end caps make only a small contribution). Rods may also be advantageous in environments where sheer forces are high, as they are able to attach to solid surfaces better than spheres. Environmental sensing (Chapter 22) may also be enhanced in elongate cells, which can have a 100 to 600-fold enhanced capacity to sense the direction of chemical gradients (Dusenbery 1998). This can be accomplished by simultaneously sensing the environment at both ends of the cell or by performing a temporal survey by swimming across and environmental gradient. Spheres are much more subject to rotational diffusion (and hence loss of directionality) than rods.

Despite the uncertainties regarding ecological and evolutionary consequences, rod-shaped bacterial cells appear to follow a specific scaling pattern such that the surface area:volume (SA:V) ratio $\simeq 2\pi V^{-1/3}$, at both the level of individual species when grown under different nutritional levels as well as at the phylogenetic between-species level (Ojkic et al. 2019). In both cases, as cell volume declines, the surface area increases, and this specific SA:V scaling requires a general mechanism to maintain the aspect ratio (length:width) at a constant value $\simeq 4$.

Although the underlying selective forces may not always be clear, cellular dimensions can undergo rapid evolutionary changes involving relatively simple modifications at the molecular level. In the case of bacteria, the molecular toolbox for cell-shape determination primarily involves two cytoskeletal molecules: the tubulin-like FtsZ, and the actin-like MreB, both noted above. For rod-shaped cells, MreB and its relatives usually play central roles in setting the cellular dimensions, directing the synthesis of the sidewalls, and operating in spatially restricted manners that ensure uniform width (Margolin 2009; Typas et al. 2012; Ursell et al. 2014). Over a period of just a few years, laboratory cultures of *E. coli* have been found to exhibit

increases in cell volume via a single mutation in the MreB gene, with further study showing that substitutions of the 20 alternative amino acids at just one amino-acid site generate a range of cell sizes, with an increase in growth rate accompanying an increase in cell volume up to a point (Monds et al. 2014). Numerous other examples exist in which simple manipulations of the protein-coding regions of these genes elicit radical shifts in cell form, e.g., spheres to rods to long filaments (Young 2010).

When MreB is deleted from rod-shaped cells, the cells generally shift to more spherical forms (Margolin 2009), and indeed bacteria that are naturally coccoid have invariably lost MreB. However, some rod-shaped bacteria have also lost MreB, implying the presence of alternative methods for the maintenance of this shape. Moreover, even when MreB is utilized in the formation of the same cell shape in different species, the end point can be achieved by rather different mechanisms. For example, the two model bacteria, *E. coli* and *B. subtilis,* both use MreB to maintain their rod shapes, but the helical movement of this molecule proceeds in a left-hand fashion in the former and a right-hand fashion in the latter. In addition, the deployment of MreB in wall growth differs, the first species regulating the amount of peptidoglycan loaded per MreB patch and the second regulating the speed of growth of individual MreB patches (Wang et al. 2012). In addition, the two species differ in the ways in which they integrate subunits into the cell wall, the thickness of which in *E. coli* is only $\sim 10\%$ that in *B. subtilis* (Billaudeau et al. 2017).

Lactococcus lactis lacks MreB and is typically an ovoid cell, but under certain environmental conditions cells can become rod-shaped, extending to long filaments. FtsZ is involved in these transformations (Pérez-Núñez et al. 2011). Generally, FtsZ directs the production of the cross-wall septum during cell division, playing a key role in cell division (Chapter 5), but in this case multiple rings of the division proteins develop along the filaments, with complete septation being inhibited. This kind of transition from spherical (coccoid) to rod-shaped cells has been seen in other bacteria (Lleo et al. 1990), but cases are also known in which shifts from rod to coccoid shapes are elicited by deletions of genes other than FtsZ and MreB (Veyrier et al. 2015). Thus, although it has been suggested that the ancestral bacterium was rod-shaped (Siefert and Fox 1998; Tamames et al. 2001), with coccoid forms being derived evolutionary dead-end states, the ease with which both types of transitions leaves little basis for such a simple interpretation.

Cell Walls

Most prokaryotes, fungi, and green plants maintain their cell shapes via external support structures such as cell walls. Other forms of structural support include the scales of haptophytes, chrysophytic algae, and other phytoplankton species (constructed from diverse substrates, including calcite, chitin, and cellulose), the silicious shells of diatoms, and the thecal plates of dinoflagellates (Okuda 2002). In addition to their roles in cell-shape determination, such outer coverings can have other roles, such as protection against pathogens and consumers. Structural support also allows aquatic cells to resist the turgor pressure that inevitably results from high intracellular molarity, which encourages the influx of water molecules from the environment. Cells lacking such pressure resistance would blow up without active

mechanisms for the continuous efflux of water. Raven (1982) makes the point that cell walls represent a one-time investment against the osmolarity problem, whereas an active mechanism of export, e.g., a contractile vacuole, incurs costs that must be paid throughout the life of the cell. Assuming negligible costs of cell-wall maintenance, the latter expense must eventually surpass the former in slower-growing cells.

One of the most striking variants of cell-wall architecture distinguishes Gram-negative from Gram-positive bacteria (originally identified by a difference in staining intensity of the cells). Bacterial cell walls are constructed primarily out of peptidoglycan (often called murein), which consists of a mesh of glycan chains linked together by short peptides. Gram-positive bacteria (also known as monoderms) have a single cell membrane surrounded by a thick cell wall, whereas Gram-negative bacteria (diderms) sandwich a thin peptidoglycan layer between two lipid membranes (often with an additional layer of lipopolysaccharides on the cell surface). Although the basic structure of peptidoglycan is universal, there is substantial variation among bacterial lineages with respect to peptide sequence, location of crosslinks between the peptide chains, and secondary modifications of the components (Vollmer and Seligman 2010).

How a dual-membrane form could have evolved from an ancestor with a single membrane (assuming this was, in fact, the ancestral bacterial state) is an unsolved problem. One idea derives from the observation that monoderms often produce double-membrane endospores. These are produced by engulfment within the maternal cell, with the plasma membrane of the mother becoming an external membrane of the spore (Vollmer 2012; Tocheva et al. 2016). Some bacteria with two membranes can also produce endospores wherein the outer membrane of the maternal cell is displaced by the inner membrane (Tocheva et al. 2011). These observations show how a cell can undergo special kinds of divisions to establish an altered cell envelope. However, such changes are terminal and lost upon spore germination, so such repatterning is a far cry from demonstrating how a stable developmental pattern of two-layer biogenesis is acquired. One interpretation of bacterial phylogeny suggests that the ancestral bacterium was a sporulating diderm (with monoderms losing the outer membrane) (Tocheva et al. 2016). If correct, this is another example of the regression of complexity to simpler forms (although it then leaves the origin of the diderm phenotype unexplained).

Like Gram-positive bacteria, the archaea nearly always have single lipid membranes, often surrounded by a variant of peptidoglycan (pseudomurein) and then by an outer crystalline shell called the S layer (Albers and Meyer 2011; Visweswaran et al. 2011; Oger and Cario 2013). S layers consist of highly organized, essentially crystalline protein lattices, with substantial variation in design among species. As there is significant variation in the biosynthetic pathways leading to murein (bacteria) and pseudomurein (archaea), and little homology between the genes involved, it has been suggested that the cell walls of these two groups evolved independently (Hartmann and König 1990; Steenbakkers et al. 2006).

Although cell walls provide obvious advantages in certain ecological settings, they have been lost in most eukaryotic and a few bacterial (e.g., *Mycoplasma* and *Ureaplasma*) lineages, presumably during prolonged periods in which the investment in biosynthesis outweighed the fitness advantages. Detailed calculations of the

bioenergetic costs of cells walls have not yet been pursued, but indirect evidence suggests that they comprise a substantial fraction of a cell's energy budget. For example, Yin et al. (2007) estimate that $\sim 21\%$ of the biomass of a *S. cerevisiae* cell consists of the cell wall ($\sim 4\%$ protein, 30% mannose, 60% glucan, and 1% chitin). The glucan subunits are derived from $\sim 7.7\times10^9$ glucose molecules, which would otherwise be available for cellular energy or as carbon skeletons for other biosynthetic pathways, and the $\sim 1.6 \times 10^6$ protein molecules per adult cell surface constitute $\sim 2\%$ of the total protein content of the cell (Klis et al. 2014). Similar numbers were obtained for another yeast species, *Candida albicans* (Klis et al. 2014).

A rough estimate of the cost of the cell wall in *S. cerevisiae* can be calculated as follows. Given that mannose is a simple derivative of a glucose molecule, and comprises half the biomass of the glucans, together these two constituents account for the equivalent of $\sim 1.5 \times 7.7 \times 10^9 = 1.2 \times 10^{10}$ glucose molecules. Noting that *S. cerevisiae* has an average cell volume $\simeq 70\ \mu\text{m}^3$, and using Equation 8.2b, the cost of building a yeast cell $\simeq 1.6 \times 10^{12}$ in units of ATP hydrolyses, or assuming that a glucose molecule is equivalent to 32 ATPs under aerobic respiration, 5×10^{10} in units of glucose molecules. Thus, mannose and glucans together account for $\sim 24\%$ of the energetic growth requirements in this species. Klis et al. (2014) further estimate that the cell wall contains $\sim 1.7\times10^6$ proteins. Assuming an average cost of synthesizing and concatenating amino acids of ~ 34 ATP hydrolyses each (Chapter 17), and an average protein length of 400 amino acids, the cost of proteins (in glucose equivalents) $\simeq 7.2 \times 10^8$, which is $\sim 1.4\%$ of the total energy budget. With the cell membrane in this species constituting an additional 4.6% of the cell budget (Chapter 17), the entire cell envelope in *S. cerevisiae* comprises $\sim 32\%$ of the total cell budget.

A similar analysis is possible for the bacterium *E. coli* (Lynch and Trickovic 2020). The basic carbohydrate subunit of peptidoglycan consists of two joined molecules, NAG (N-acetylglucosamine) and NAM (N-acetylmuramic acid), with short peptide chains fused to the latter for cross-bridging. Using methods outlined in Chapter 17, the total cost of synthesis of each peptidoglycan unit can be shown to be equivalent to ~ 209 ATP hydrolyses, and there is an estimated 3.5×10^6 disaccharides in the entire cell wall (Wientjes et al. 1991; Gumbart et al. 2014), implying a total cost of $\sim 7.3 \times 10^8$ ATP hydrolyses ($\sim 2.7\%$ of the total cell-growth budget). In the *E. coli* envelope, there are also $\sim 10^6$ molecules of Braun's lipoprotein (Li et al. 2014; Asmar and Collet 2018), which attaches the outer membrane to the cell wall. Each of these molecules consists of a chain 58 amino acids (worth ~ 34 ATPs each, including chain elongation) and three chains of palmitate (~ 122 ATPs each) for a total cost of 2338 ATPs per unit, and $\sim 2.3\times10^9$ ATPs in total, or $\sim 8.5\%$ of the total cell budget. There are in addition $\sim 1.2\times10^6$ lipopolysaccharide molecules on the surface of the cell (Neidhardt et al. 1990), with a cost of 1048 ATPs per molecule, accounting for another 3.6% of the cell's construction budget. Finally, the total cost of lipids in the cell membranes of *E. coli* comprises $\sim 34\%$ of the cell budget (Chapter 17). Thus, summing all of these components, the entire envelope constitutes $\sim 49\%$ of the energy budget of an *E. coli* cell. This is a downwardly biased estimate, as the considerable costs of surface antigens attached to the ends of lipopolysaccharides (and present in variable amounts in different strains) have been ignored.

Extension of this sort of analysis to the Gram-positive bacterium *B. subtilis*

leads to the conclusion that, despite the membrane organization differences from *E. coli,* about a third of the total-cell energy budget is allocated to the envelope, with $\sim 25\%$ of the latter being associated with the thickened cell wall (Lynch and Trickovic 2020). Thus, for species with cell walls, lipid membranes are generally still the most expensive components of the envelope. Most significantly, however, the overall cost of the envelope constitutes a larger fraction of a cell's energy budget than any other single component, although this declines with increasing cell volume as a consequence of the reduction in surface area:volume ratio (Chapter 17).

A wide variety of wall types exists in eukaryotes. One macro-scale classification uses categories related to whether walls are internal or external to membranes, neither, or both (Becker 2000), although such a scheme belies the underlying diversity in chemical makeup (Niklas 2004). One of the most common constituents of eukaryotic cell walls is cellulose, a linear polymer of glucose residues, which may be the most common biomolecule in the world. Found throughout plants, some slime molds, some bacteria, and even a group of animals (tunicates), this simple molecule does have variants among phylogenetic lineages, with the glucosyl residues sometimes carrying modified side chains.

The phylogenetic distribution of cellulose biosynthetic capacity, along with the conserved structure and sequence of the underlying machinery, strongly suggests its movement into and throughout eukaryotes by horizontal transfer events, possibly starting with the endosymbiotic colonist that formed the chloroplast. It remains a mystery, however, as to why eukaryotes have completely abandoned the use of peptidoglycans, if they ever had them. Biosynthesis of peptidoglycan in bacteria starts with UDP-acetyl glucosamine, whereas cellulose biosynthesis starts with UDP-glucose, implying either an ancient common ancestry for the production of such building blocks, or another case of convergent evolution.

Contrary to the situation with bacterial peptidoglycan held together by peptide cross-linking, cellulose consists of long aggregated filaments of the underlying glucose derivatives held together by intra- and inter-chain hydrogen bonds. Cellulose production proceeds in a spatially organized fashion via large, membrane-bound cellulose synthase complexes, organized in rows, arrays, or rosettes in different species, with the organizational form defining the dimensions of the resultant microfibrils and their aggregated mesh-like forms (Niklas 2004; Saxena and Brown 2005). Based on the known biosynthetic pathway, the cost of each glucan subunit is equivalent to ~ 34 ATP hydrolyses, although it remains an open question as to the total investment cells make in cellulose (which requires estimates of the total number of subunits per wall).

In seemingly no case do walls consist solely of cellulose, with a wide variety of glycoproteins, lignins, pectins, uronic acids, xyloglucans, and many others being utilized in various forms of cross-linking in individual lineages (Niklas 2004; Domozych et al. 2014). In the brown algae, cellulose is a relatively minor component of cell walls, the majority consisting of other forms of linked polysaccharides called alginates and sulfated fucans thought to have been acquired by horizontal transfer from bacteria (Michel et al. 2010). Even rough estimates of the costs of these components would be useful. As one example, deposition of silicon into the frustules of diatoms may be relatively cheap, involving the expenditure of perhaps just a single ATP per incorporated molecule, with the total cost to a cell being only $\sim 2\%$ of the

total energy budget (Raven 1983), although this ignores the underlying organic wall components.

Molecular Motors

In prokaryotes, most intracellular molecular transport is passive, driven primarily by random diffusion resulting from background thermally induced molecular motion. In eukaryotes, however, a good deal of molecular transport comes at a cost, in particular active transport driven by ATP-consuming molecular motors, with diverse functions ranging from cargo transport along actin filaments and microtubules to the movement of flagella (Howard 2001). Actins and tubulins can exert mechanical pressure on their own, as they push against larger structures, and thermal fluctuations allow the stochastic insertion of monomeric subunits and progressive extension. However, motor proteins supplement the cytomotive capacity of the cytoskeletal filaments, using them as highways for dragging along attached cargoes (Figure 16.2).

Given their apparent absence from prokaryotes, all three major families of cytoskeleton-associated motors – dynein, kinesin, and myosin – likely emerged on the path between FECA and LECA. Myosins travel exclusively on actin filaments, whereas kinesins and dyneins operate on microtubules (tubulin filaments). Their physical structures vary, but each type of molecule works by the same mechanism – the transduction of chemical energy into mechanical force via ATP hydrolysis. Each motor molecule has an ATP-binding site, a track-binding site, and a tail domain involved in cargo attachment. Although the specific details remain unclear (Hwang and Karplus 2019), the molecules effectively walk along their cytoskeletal roadways, with each ATP hydrolysis resulting in one step forward (in some cases two hydrolyses occur per step; Zhang et al. 2015).

Ubiquitous to all eukaryotes, kinesins underwent massive diversification into an estimated eleven families prior to LECA (Lawrence et al. 2004; Richards et al. 2004; Wickstead et al. 2010). Prominent roles include vesicle transport, spindle assembly, chromosome segregation, and intraflagellar transport of flagellar components. Monomeric, dimeric, trimeric, and tetrameric forms exist, and the multimers may be either homomeric or heteromeric. The motor domains generally operate like walking feet paired together at one end of the molecular structure, although tetramers have motor domains on both ends. Kinesin movement is generally unidirectional, towards the + ends of microtubules (usually moving from the center to the edges of cells), with typical rates of movement on the order of 0.5 to 1 μm/sec and stride lengths $\simeq$ 8 nm (Block et al. 1990; Howard 2001; Muthukrishnan et al. 2009; Scholey 2013). However, those involved in meiosis and mitosis are particularly slow, with speeds on the order of 0.05 μm/sec. Different kinesins vary in neck lengths, and these and other molecular features determine the degree of processivity of the motors along tubulin filaments (Hariharan and Hancock 2009; Shastry and Hancock 2010; Cochran 2015).

Myosins are nearly ubiquitous among eukaryotes, but apparently have been lost from the red algal, diplomonad, and trichomonad lineages (Richards and Cavalier-Smith 2005; Foth et al. 2006). Although myosins and kinesins differ in size and exhibit little sequence similarity, they may have evolved from a common ancestor,

given the similar 3-D structures of their functional domains (Kull et al. 1998). The most likely ancestral state prior to eukaryotic diversification is something on the order of three myosin classes, all derived from a single common ancestral protein en route from FECA to LECA. However, like kinesins, myosins further diversified into a large number of subclasses (as many as 24; Foth et al. 2006; Goodson and Dawson 2006), again with numerous functions, including cellular motility, and transport of organelles, vesicles, and mRNAs. An argument has been made that diversification of myosin functions followed paths of subfunctionalization, from generalized to more specialized forms (Mast et al. 2012), with the original functions involving cytokinesis, vesicle transport, phagocytosis, and locomotion by pseudopods.

Although most myosins are dimeric with parallel coiled-coil domains, monomeric forms exist, as do dimers with anti-parallel constructs with actin-binding domains at each end (Quintero and Yengo 2012). Almost all myosins move in the + direction of actin filaments, although a few are known to move in the opposite direction. Each type of molecule has a specific affinity for filaments and a particular step length (usually 5 to 40 nm per step), and speeds often in the range of 0.3 to 0.5 μm/sec, which together determine the speed of movement (Elting et al. 2011). However, a myosin involved in cytoplasmic streaming in plant cells can move at rates up to 60 μm/sec (Titus 2016). Exceptionally high rates occur when myosins run rather than walk, jumping from point to point with actual step lengths greater than those that can be accomplished when one motor domain is always in contact with the filament.

Dyneins, the third major class of motor proteins, have a substantially different structure than kinesins and myosins, including an intramolecular hexameric ring consisting of AAA (ATPases Associated with cellular Activities) domains, all physically linked in a single gene (Kardon and Vale 2009). Containing > 4500 amino-acid residues, dyneins are among the largest known proteins. In total, there are at least nine deeply diverging dynein lineages, most of which trace back to LECA, although they were independently lost in the lineages leading to land plants and red algae. Although dyneins maintain the attribute of having two walking feet, with each step fueled by single ATP hydrolysis, contrary to the situation with kinesins, dyneins always walk towards the $-$ ends of microtubules, typically towards the cell center, and with variable speeds in the range of those noted above (Walter and Diez 2012; Sweeney and Holzbaur 2016). Dyneins are also unique in that all but one cytoplasmic family member is associated with the cilium (Wickstead and Gull 2007; Wilkes et al. 2008). The latter operate in a team-like fashion to elicit ciliary movement, causing microtubules to slide past each other.

Although molecular motors have been subject to numerous biochemical and biophysical studies, few questions have been asked from an evolutionary perspective. The three central phenotypic features of motor proteins are their step length, step rate, and processivity (distance progressed before falling off a substrate). Although all three parameters are readily estimated in laboratory constructs, and the rate of movement is equal to the product of the length and rate of steps, almost nothing is known about how these traits vary among species or among motor family members within species. In addition, the total drain on a cell's energy budget owing to motor activity is essentially unknown.

Motility

All cells are capable of movement, even if simply as a consequence of the physical forces associated with cell division. Here, however, the concern is with active movement within the lifespan of a cell, as in swimming or crawling. The range of cellular motility mechanisms is diverse, and even seemingly similar, complex mechanisms such as flagella have evolved independently in different lineages. Regardless of the mechanism, all forms of motility require some investment of energy, either a gradient of hydrogen ions driving a turbine-like apparatus or active hydrolysis of ATP used in the conversion of chemical to mechanical energy used in microfibril movement. In addition, the construction of the motility machinery itself can require a substantial energetic investment. Thus, unless active motility provides a boost in fitness, the mechanism will be liable to rapid loss, as this can free up substantial energy for other cellular functions.

The details of how simple cells can utilize mechanisms of directed motion to enhance resource acquisition will be addressed in Chapter 18, with the primary focus here being on the evolutionary origins of motility machineries and the costs of running and building them. Flagella and cilia have received considerably more attention than mechanisms of crawling, and accordingly are given the most attention in the following sections.

Crawling in eukaryotes. Numerous bacteria are capable of movement on solid surfaces (Jarrell and McBride 2008; Nan and Zusman 2016). For example, some bacteria, such as *Neisseria,* can crawl over surfaces by twitching of Type IV pili, whereas others, such as the social bacterium *Myxococcus,* glide by use of surface adhesins (either secreted or embedded in the membrane), and still others move by an inchworm-like mechanism involving membrane-embedded proteins. In addition, crawling is achieved by similar enough molecular mechanisms over diverse phylogenetic groups of eukaryotes that there seems little doubt that LECA was capable of such movement (Fritz-Laylin et al. 2017). Moreover, given that a similar conclusion has been reached on the origins of the eukaryotic flagellum (below), and the fact that numerous eukaryotic lineages have cells capable of both flagellar swimming and amoeboid movement (Fulton 1977; Brunet et al. 2021; Prostak et al. 2021), LECA was likely capable of both forms of motility, unless crawling has evolved independently by similar mechanisms. If correct, this would also suggest that LECA was devoid of a cell wall which would prevent the production of cytoplasmic extrusions necessary for crawling.

Despite the approximate uniformity of mechanisms, most notably the shared use of actins and actin-associated proteins to generate growth and retraction of cellular protrusions, a variety of structures are used in crawling activities. These can generally be classified into two major groups: 1) pseudopods, which involve broad protrusions underlain by branched actin-networks, and allow cells to drag themselves across surfaces; and 2) filopods, which involve narrower and linear extensions of unbranched actin bundles that enable a more walking-like motion. Unlike more permanent flagella, all such structures are dynamic, allowing rapid changes in shape via local assembly and disassembly of the underlying cytoskeleton. In addition, blebs produced in some lineages involve cytoplasmic extensions of the cell surface released from the underlying actin cortex. One of the primary side activities associated with crawling is the ingestion of food particles by phagocytosis.

In general, crawling on surfaces proceeds at much lower speeds than swimming through liquids. For example, the amoeba *Naegleria gruberi* crawls at a rate of 1 to 2 μm/sec (Preston and King 2003, which is one to two orders of magnitude more slowly than typical swimming speeds for prokaryotes and eukaryotes of similar size (below). Gliding motility in *Myxococcus* is even slower, on the order of 0.03 μm/sec (Tchoufag et al. 2019).

Based on the cost of actin polymerization, Flamholz et al. (2014) estimated that the crawling motion in goldfish keratocytes consumes $\sim 4 \times 10^5$ ATPs/second. Recalling from Chapter 8 that the basal metabolic requirement of a vertebrate cell $\simeq 5 \times 10^7$ ATPs/second, and that, assuming a one-day cell division time, the cost of building such a cell is $\sim 6 \times 10^8$ ATPs/second, the cost of crawling in this particular case is on the order of 1% of such a cell's operational budget (or $\sim 0.1\%$ of the total energy budget).

Prokaryotic flagella. Some planktonic cyanobacteria, such as *Synechococcus,* can swim without flagella (Waterbury et al. 1985), and others are capable of buoyancy regulation via gas vacuoles (Walsby 1994), but the vast majority of bacterial swimming involves a flagellum, one of the most complex molecular machines within bacterial cells (Figure 16.3). The dozens of proteins contributing to the overall structure can roughly be divided into five major components: the basal body (which includes the membrane-embedded stator within which the motor rotates), the switch, the hook, the filament, and the export apparatus. Bacterial flagellar assembly starts at the basal body, anchoring the overall structure to the cell membrane, proceeds to the construction of the hook, and finally to the filament. The latter is a hollow, tubular structure, consisting of tens of thousands of flagellin molecules, making this one of the most abundant proteins in swimming bacterial cells. Its assembly proceeds by the export of component proteins through a central pore. Specific chaperones are assigned to each exported protein, which have to remain unfolded until passing through the pore. The monomeric flagellin subunits are then configured in such a way that the final structure is helical in form. Unicellular species live in a low Reynold's number world (Foundations 16.2), where viscous forces dominate to the extent that there is essentially no inertia upon cessation of activity. Thus, rather than pushing the cell forward like legs or wings on an animal, bacterial flagella essentially operate like cork screws, pulling the cell forward through an effectively syrup-like environment.

Generally driven by a proton-motive force (but in some species, by a sodium-motive force or even by divalent cations; Ito and Takahashi 2017), the helical filament rotates within the hub embedded in the cell membrane (Manson et al. 1977, 1980; Meister et al. 1987), much like a rotor guided by a surrounding stationary stator in an electrical motor (and not unlike the situation with ATP synthase; Chapter 2). Although the bacterial flagellum does not directly consume ATP, an ATP-driven proton pump maintains the gradient of hydrogen ions necessary to run the turbine. Energy associated with ions passing through channels surrounding the motor is converted to a rotational force, which is applied to the internal shaft, analogous to the links of a bicycle chain rotating a wheel. The speed and orientation can be regulated through various signal transduction systems (Chapter 22) that modify flagellar activity (Boehm et al. 2010).

Despite the intricacies of the bacterial flagellum, there is substantial phylogenetic variation in its basic features, including the angularity and periodicity of the helices, clockwise vs. counter-clockwise rotation of the helices (or both), the number of distinct flagellin proteins incorporated into the filament, and the number of protofilaments per flagellum (Pallen and Matzke 2006; Galkin et al. 2008; Chaban et al. 2018; Kaplan et al. 2019). Enormous variation also exists in the structure and number of components in the basal body (Chen et al. 2011; Moon et al. 2016; Chaban et al. 2018; Rossmann and Beeby 2018). The cellular positions and numbers of flagella are also highly variable. Although the flagella of most bacteria are not surrounded by membranes, in numerous genera, including *Helicobacter, Vibrio,* and *Bdellovibrio,* they are (Seidler and Starr 1968; Geis et al. 1993; Zhu et al. 2017). In spirochaetes, the flagella are not even external, but reside within the periplasmic space, where their twisting contorts the entire cell. The degree to which the scattered presence of flagella throughout the bacterial phylogeny is due to lineage-specific losses or gains by horizontal gene transfer remains unclear (Snyder et al. 2009).

How might a molecular machine as complex as a bacterial flagellum have arisen? That paths of descent with modification are involved is supported by several lines of evidence. For example, the subcomponent that drives flagellar component export is related to the catalytic subunits of ATP synthase. In addition, the remainder of the system appears to be related to cell-surface projections used to transfer infection-determining proteins into host cells, so-called Type-III secretion systems (Pallen et al. 2005). At least ten components of such secretion systems have strong homologies to components of the bacterial flagellum, and the overall architecture is similar. The main difference is that instead of a flagellum, the secretion system harbors a stiff injection apparatus (Blocker et al. 2003; Egelman 2010).

Liu and Ochman (2007) provide evidence that least 24 of the > 50 genes whose products enter the bacterial flagellar system were likely present in the common ancestor to all bacteria, and that many of the component origins involved gene duplication. They further suggest that the order of inferred duplications imply an "inside-out" sequence of evolutionary steps that in turn reflects the assembly process, i.e., basal body, hook, junction, and filament, a potential example of ontogeny recapitulating phylogeny. These observations provide further support for the idea that the flagellum arose from something like a Type-III secretion system, rather than the other way around. Nonetheless, just as the flagellum may have evolved from bacterial structures with alternative functions, partial loss of the flagellum sometimes leads to the maintenance of structures with novel functions. For example, *Buchnera aphidicola,* an endosymbiont that inhabits the cells of aphids, has lost the flagellar filament, but the cells still harbor hundreds of hook/basal body structures, with likely roles in secretion into host cells, much like Type-III secretion systems (Maezawa et al. 2006; Toft and Fares 2008).

Although fairly similar in overall structure, the flagella of archaea appear to be completely unrelated to those of bacteria, providing a remarkable example of convergent evolution. As in bacteria, the archaeal flagellum (the archaellum) rotates via an embedded membrane structure. However, rather than being driven by a proton-motive force, ATP hydrolysis drives rotation of the archaellum (Thomas et al. 2001; Desmond et al. 2007; Lassak et al. 2012; Daum et al. 2017; Albers and

Jarrell 2018). The components of the whip, archaellins, appear to be unrelated to bacterial flagellins, and unlike the situation in bacteria, archaeal flagella are not hollow and have no hook structure. Archaeal flagella appear most closely related to bacterial type IV pilus systems (Albers and Pohlschröder 2009), which are used as adhesive structures and in twitching motility, although this too might be a matter of convergence.

Eukaryotic flagella. This theme of diversity extends to the eukaryotic flagellum, which is unlike anything utilized in the prokaryotic world. Unlike the rotational flagella of prokaryotes driven by a proton-motive force, eukaryotic flagella operate by a whip-like mechanism driven by ATP-consuming motor proteins, which cause doublets of microtubules to slide past each other. Only a few eukaryotic lineages lack the ability to produce flagella, most notably slime molds, yeasts, and land plants, leading to the general conclusion that the origin of the eukaryotic flagellum preceded LECA (Cavalier-Smith 2002; Nevers et al. 2017). In some protists, such as ciliates and barabasalids, an enormous proliferation of proportionally short flagella coats large portions of the cell surface. The word cilia (singular cilium) is generally reserved for these cases, although aside from length differences relative to cell size, the basic structure remains the same.

As in bacteria, there are many variants on the structure and deployment of eukaryotic flagella. For example, the green alga *Chlamydomonas* can swim either by a breaststroke or by undulatory waves (Tam and Hosoi 2011). The cryptophyte *Ochromonas* has perpendicular hairs (mastigonemes) radiating from the flagellum, creating a feather-like appearance. Combined with the use of flagella, euglenoids are capable of additional cell contortions (called metaboly), with the cell shifting the positions of cellular contents progressively along its axis (like food moving through an animal's gut). In trypanosomes, a single flagellum is embedded along the side of the cell.

Eukaryotic cilia are much larger than bacterial flagella, generally on the order of 200 nm in diameter as compared to 10 to 30 nm in prokaryotes, and almost always consisting of bundles of nine peripheral microtubule doublets surrounding a central pair (Ginger et al. 2008; Ishikawa and Marshall 2011, 2017). (The central pair is typically absent in derived structures called primary cilia, which are used as sensing organs in cells of metazoa). This overall core structure, known as an axoneme, is surrounded by an extension of the cell membrane. The doublets grow out of cylinders known as basal bodies, where the microtubules consist of triplets comprised of δ- and ϵ-tubulins, which arose by gene duplication prior to LECA (Dutcher 2003). In most organisms, the basal bodies are recycled centrioles, which are also used as mitotic-spindle organizing centers during cell division (discussed above).

While bacterial flagella are comprised of a few dozen proteins, on the order of 250 to 500 proteins contribute to the eukaryotic flagellum, up to 3% of the proteins encoded in a eukaryotic genome (Avidor-Reiss et al. 2004; Pazour et al. 2005; Smith et al. 2005). For the few organisms for which the flagellar proteome has been evaluated (the green alga *Chlamydomonas,* the ciliate *Tetrahymena,* and mammals), ~ 200 proteins are flagellar-specific and not found in nonciliated species (Avidor-Reiss et al. 2004; Smith et al. 2005).

Numerous activities occur within the lumens of eukaryotic flagella, which are in a constant state of assembly and disassembly at the tip. As there are no ribosomes within the flagellum, all materials must be selectively imported by intraflagellar transport (IFT). However, eukaryotic flagella contain metabolic machinery for generating ATPs that are presumably used to fuel the molecular motors involved in transport and motility (Ginger et al. 2008). Kinesins move structural and other flagellar components forward on one member of each microtubule doublet, while dyneins move cargo in the opposite direction on the other member (Stepanek and Pigino 2016), preventing bi-directional traffic collisions. Transport rates are on the order of 1 to 3 μm/sec (Ishikawa and Marshall 2017). Flagella also function secondarily as sense organs, harboring numerous signal-transduction systems (environmental sensors that initiate information cascades within cells; Chapter 22).

The most convincing scenario for the evolution of the eukaryotic flagellum invokes an autogenous origin, starting as protruding microtubule bundle emanating from a microtubule organizing center (as used in mitotic spindles) (Cavalier-Smith 1978; Jékely and Arendt 2006). Such an initial structure may have had little to do with motility at all, operating instead as an environmental sensing organ. Eventually an IFT system would have to evolve, along with the ninefold symmetric structure of the axoneme, and the recruitment of molecular motors. Such a scenario invokes little more than a series of gene duplication and modification events associated with tubulins and motors deployed in the cellular interior (Hartman and Smith 2009). An alternative hypothesis, which postulates an origin via a virus that somehow victimized a host cell in such a way as to produce a primitive basal body for extruding viral particles (Satir et al. 2007; Alliegro and Satir 2009), has an obvious problem of ignoring the cost of maintaining such a pathogen for the eons required for the emergence of the complex ciliary structure.

Further potential insight into the origins of the components of the eukaryotic flagellum derives from similarities to various structural and functional aspects of the nuclear pore complex and vesicle scaffolding proteins. Fibers at the base of the flagellum may operate as gateways to admission of appropriate protein cargoes for intraflagellar transport, making use of RAN-GTP cycles and importin molecules as in the case of transport through nuclear pores (Rosenbaum and Witman 2002; Dishinger et al. 2010; Kee et al. 2012; see Chapter 15). Notably, the two IFT protein complexes that bind to cargoes (and are in turn dragged by motors) appear to be derived by duplication from a common ancestor related to vesicle-coat proteins (van Dam et al. 2013), which as noted in Chapter 15 are in turn related to the scaffold of the nuclear pore complex. Left unresolved here is whether the nuclear-pore complex preceded the evolution of the flagellum or vice versa, but these observations again illustrate how the complex features of cells often evolve by duplication and modification of pre-existing structures rather than by *de novo* establishment.

The eukaryotic flagellum has also served as a model for understanding how size homeostasis is maintained for cellular organelles, one of the key questions in developmental biology focused at the cellular level (Chapter 9). Inappropriate flagellum lengths (including unequal lengths in species with paired flagella) lead to aberrant swimming patterns (Tam et al. 2003; Khona et al. 2013). Because eukaryotic flagella undergo constant assembly and disassembly of tubulin subunits (Marshall and Rosenbaum 2001), maintenance of a constant length implies that the two rates

equalize. This further requires that at least one of the two reaction rates be length-dependent, such that disassembly exceeds assembly above the equilibrium length, and vice versa below the equilibrium. Such regulation is supported by experiments in the biflagellated *Chlamydomonas,* showing that when one flagellum is severed, it grows back while the other shrinks until the two equilibrate in length (Ludington et al. 2012, 2013). One suggestion for such behavior is that the rate of assembly declines with cilium length as the arrival time of tip components by IFT declines with the distance that must be traveled by each particle (Ludington et al. 2013). However, the data appear to support an active-disassembly model, with depolymerization increasing with flagellum length (Fai et al. 2019). In the case of *Giardia,* which has four pairs of flagella of different lengths, the data again support a model of length-independent assembly and length-dependent disassembly associated with the behavior of kinesins (McInally et al. 2019).

The costs of swimming. Although many cells can swim, and it is easy to imagine adaptive reasons for doing so, e.g., directive movement towards patchy resources and avoidance of predators, not all cells living in aquatic environments can self-propel. The latter include many planktonic bacteria, diatoms, and green algae. This suggests that the energetic cost of swimming in certain settings may exceed the benefits. Drawing from prior work (Lynch and Trickovic 2020), an effort is made here to obtain a rough estimate of such costs for both the act of swimming and of building the mobility apparatus, and to determine how the evolutionary consequences of such costs scale with cell size.

The baseline power requirement for swimming can be estimated as the work required to move an object (usually assumed to be a sphere, or an alternatively shaped cell suitably transformed to an effective sphere) at a particular velocity (Foundations 16.2). In biology, the mechanical force essential for movement is obtained by a conversion from chemical energy, i.e., ATP hydrolysis, which is a less than perfect process. Comparing the predictions of physical theory with actual estimated costs of moving flagella, a number of attempts have been made to estimate the efficiency of swimming in microbes. The universal conclusion is that the conversion of chemical energy into motion is quite low, averaging $\sim 1\%$: $\sim 0.1\%$ for the ciliate *Paramecium* (Katsu-Kimura et al. 2009); 1.3% for the euglenoid *Eutreptiella* (Arroyo et al. 2012); 0.8%, 1.5%, and 1.4%, respectively, for the green algae *Chlamydomonas* (Tam and Hosoi 2011), *Polytoma uvella* (Gittleson and Noble 1973), and *Tetraflagellochloris mauritanica* (Barsanti et al. 2016); 8% for the archaebacterium *Halobacterium* (Kinosita et al. 2016); and 1% and 5%, respectively, for the bacteria *E. coli* (Purcell 1977; Chattopadhyay et al. 2006) and *Streptococcus* (Meister et al. 1987). Thus, the power requirement for swimming is on the order of $100\times$ that expected based solely on the physics of the process. Brownian-motion jostling of cells, rotational diffusion, helical swimming patterns, and flexibility of the flagellum are among the reasons for this low efficiency.

Despite this low efficiency, it has been suggested that the total cost of swimming is still trivially small (Purcell 1977), but this sort of statement needs context. Only a few attempts have been made to estimate the cost of swimming. Raven and Richardson (1984) concluded that the cost of running a flagellum for an idealized dinoflagellate is about equal to the basal metabolic rate, whereas Katsu-Kimura et

al. (2009) suggested 70% for the ciliate *Paramecium*. Crawford (1992) estimated that 1 to 10% of ciliate and dinoflagellate total energy budgets are allocated to swimming, whereas Fenchel and Finlay (1983) estimated costs equivalent to $\sim 0.4\%$ of total cellular energy budgets in the cryptomonad *Ochromonas* and the ciliate *Didinium*.

There are a number of uncertainties in this broad range of estimates, and notably, they ignore the cost of building the apparatus required for motion. Nonetheless, although fractional energy investments as low as 0.1 to 1% may seem trivial in an absolute sense, this is not correct from an evolutionary perspective, as such a cost can easily be perceived by natural selection in most populations. As discussed in Chapters 4 and 5, the power of selection is almost always sufficient to perceive a cost as low as 0.01% (and much lower than that in unicellular species). Thus, it is clear that the cost of swimming is sufficiently large that such a trait exists in an evolutionary "use it or lose it" context, with promotion of nonmotile mutants likely if the benefits of motility do not exceed the cost of operation.

A more general view of the problem can be obtained from the scaling relationship between swimming velocity (v in units of μm/sec) and cell volume (V in units of μm^3) (Figure 16.4). For eukaryotic species, average $v \simeq 16.6V^{0.25}$, and noting that the radius of a sphere is $r = (3V/4\pi)^{1/3}$, this suggests a swimming speed for unicellular eukaryotes of $\sim 13V^{-0.08}$/sec in units of effective cell diameters ($2r$), yielding average estimates near 4 and 13 lengths/sec for the largest ($V = 10^6$) and smallest ($V = 1$) swimming cells. Some ciliates are capable of "jumping" behavior at rates of 130 to 150 lengths/sec (Gilbert 1994). Scaled in this way, swimming speeds for eukaryotic cells are comparable to those observed for the larvae of marine invertebrates, which generally fall in the range of 5 to 10 lengths/sec (Chia et al. 1984), and much higher than those for swimming vertebrates (fish, birds, seals, and whales, all of which fall in the narrow range of 0.5 to 2.5 m/sec; Sato et al. 2007). The peak speeds of the fastest fish (marlins and sailfish) are ~ 15 body lengths/sec, and the maximum speed for an Olympic swimmer is ~ 2 body lengths/sec.

When the same derivation is made for bacteria, average swimming speeds in units of cell length are found to be $\sim 24V^{-0.16}$/sec, yielding average estimates of 17 and 35 lengths/sec for the largest ($V = 10$) and smallest ($V = 0.1$) swimming bacterial cells. In this sense, despite their small size and simplicity, bacteria are easily the champions of the swimming world.

How much energy does such activity demand? From Equation 16.2.2, it can be seen that the power required for swimming scales with the product of the viscosity of the medium (η), the radius of the cell (r), and the squared swimming velocity (v^2), and to account for the inefficient conversion from chemical energy to motion, this must further be multiplied by 100 (from above). Assuming spherical cells, the scaling relationship for eukaryotes in Figure 16.4 implies $rv^2 \simeq 171V^{0.83}$ $\mu\text{m}^3/\text{sec}^2$. From Chapter 3, the viscosity of water is 10^{-2} g $\cdot$ cm^{-1} $\cdot$ sec^{-1} (assuming 20° C), and after applying this to Equation 16.2.2 and appropriate changes of units, the average power requirement of swimming is estimated to be $(1.6 \times 10^{-16})V^{0.83}$ kg $\cdot$ m^2 $\cdot$ sec^{-3}, which has equivalent units of joules/sec (here, cell volume V is in units of μm^3).

To put this in more familiar terms, note that a rough estimate of the energy associated with the hydrolysis of one mole of ATP at physiological conditions is

50 kilojoules. After allowing for Avogadro's number of molecules per mole, the power requirement for swimming in units of ATP molecules hydrolyzed/hour is then $\sim (17 \times 10^6)V^{0.83}$ for eukaryotes, and similar extrapolation leads to $(54 \times 10^6)V^{0.67}$ for bacteria. Recalling that average basal metabolic rates scale isometrically with cell volume, $\simeq 0.4 \times 10^9 V$ ATP hydrolyses/hour at 20° C (Chapter 8), this suggests a fractional energetic investment in swimming (relative to total maintenance costs, and assuming the cell is constantly swimming) in the range of 1 to 4% for the largest and smallest eukaryotic cells, but substantially higher in bacteria, ranging from 6% in the largest to 29% in the smallest swimming species.

These estimates do not include the cost of building the swimming apparatus. As outlined in Foundations 16.3, the total biosynthetic cost of the proteins comprising each *E. coli* flagellum and its basal protein parts is equivalent to $\sim 10^8$ ATP hydrolyses. The flagella of some bacteria are surrounded by a lipid membrane, and although *E. coli* is not one of them, were it to do so, the cost would be $\sim 3.6 \times 10^8$ ATP hydrolyses, raising the total construction cost by $\sim 5\times$ relative to that for a naked flagellum.

Although approximations, such calculations motivate some conclusions with respect to swimming in bacteria. First, recalling from above that the cost of swimming is $\sim (54 \times 10^6)V^{0.67}$ ATP hydrolyses per hour for bacteria, because the average volume of an *E. coli* cell is $V \simeq 1$ μm^3, the cell-division time is typically no more than a few hours, and an average cell harbors several flagella, more than 50% of the cost of swimming will typically be associated with building as opposed to operating the apparatus. Second, from Chapter 8, the total cost of building an *E. coli* cell is $\sim 2.7 \times 10^{10}$ ATP hydrolyses, implying that the bioenergetic cost of building each flagellum is on the order of 0.4% of the total cellular energy budget. There will, of course, be quantitative differences among species after variation in flagellar lengths and numbers and cell size are accounted for, but given that most swimming bacterial cells, including *E. coli,* have multiple flagella, the total construction cost of flagella will typically exceed 1% of the cell's total construction budget.

Calculations for eukaryotes (Foundations 16.3) suggest roughly similar relative costs of swimming. Noting that the volume of a *C. reinhardtii* cell is ~ 150 μm^3, and allowing for a 24-hour cell division time implies an energetic cost of swimming of $\sim 2.6 \times 10^{10}$ ATP per cell life time, whereas the costs of flagellar construction are $\sim 3 \times 10^{10}$ ATP hydrolyses for the protein content and $\sim 10^{10}$ for the lipid membrane (for each of the two flagella). With the total cost of building a *C. reinhardtii* cell being $\simeq 3.2 \times 10^{12}$ ATP hydrolyses (Chapter 8), the relative costs of swimming and constructing the flagellar pair are 0.8 and 2.5%, respectively.

Thus, from an evolutionary perspective, it can clearly be concluded that the cost of swimming constitutes a significant fraction of a cell's total energy budget. In accordance with this view, many bacteria have evolved mechanisms for selective use of flagella, regulating the expression of the necessary genes for use only in environments providing significant benefits. When confronted with nutrient depletion, some species shed all external features of their flagella, leaving behind just a plugged remnant of the flagellar motor, whereas others cease assembly, leading to a reduction in flagellum number as the cells divide (Ferreira et al. 2019).

Prolonged periods of silencing of such genes would be expected to eventually lead to the accumulation of deactivating mutations (and complete loss of motility),

and this presumably explains the absence of flagella/cilia from numerous branches in the Tree of Life. Once such an event occurs, there must also eventually be a point at which mutation accumulation is so high that reversion to motility is impossible without horizontal gene transfer. However, a remarkable case of the resurrection of a flagellum was observed in an experimental construct of the bacterium *Pseudomonas fluorescens* engineered to be nonmotile by deletion of a key regulatory gene for flagellar gene expression (Taylor et al. 2015). After just four days of strong selection for motility, the bacteria regained flagella as mutations redirected a regulatory gene for nitrogen assimilation towards the promotion of expression of still intact flagellar genes (albeit at the expense of nitrogen uptake).

Summary

- Eukaryotic cells rely heavily on protein polymers consisting of monomeric (actin) or heterodimeric (tubulin) subunits to construct linear beams used in a variety of cellular functions ranging from structural support to intracellular trafficking and motility.

- Although less apparent at the cellular level, evolutionary relatives of such filaments are also found in prokaryotes, implying their presence at the time of the last universal common ancestor, with subsequent functional modifications arising in the eukaryotic domain. In particular, shifts in the deployment of tubulins vs. actins for different functions between the major domains of life provide dramatic examples of convergent evolution of cellular functions at the molecular level.

- Scaled to the total costs of constructing cells, the investment in fibrillar proteins in eukaryotes ($\simeq$ 0.1 to 2%) may be only two-fold greater than it is in prokaryotes.

- Cell sizes and shapes are sustained by endoskeletons (fibrillar proteins) and/or exoskeletons (cell walls). Although the detailed genetic mechanisms underlying cell-shape homeostasis and the evolutionary mechanisms driving shape changes are largely unknown in eukaryotes, in bacteria, substantial shifts in the geometric features of cells can be accomplished by just single amino-acid changes in one or two proteins.

- Many species deploy hard cell coverings, either internal or external to the plasma membrane, which resist turgor pressure and likely have other functions such as avoiding predation. Although peptidoglycans (prokaryotes), and glycans, cellulose and chitin (eukaryotes) are common components of cell walls, numerous variants are deployed across eukaryotic phylogeny, including the use of inorganic components (e.g., silicon and calcium) in some lineages.

- The investment in cell walls can be quite substantial, accounting for as much as half the costs of the complete cell envelope, with the latter (including lipid membranes) comprising on the order of 20 to 40% of a cell's lifetime energy budget. These numbers are strikingly similar to the rule-of-thumb that one should spend no more than one-third of one's income on a home.

- Whereas most intracellular transport in bacteria relies on passive diffusion, eukaryotic cells deploy molecular motors to carry large cargoes, such as vesicles, using the cytoskeleton as a structural highway. Three major classes of molecular motors exist within eukaryotes (kinesins, myosins, and dyneins), all of which diversified into multiple subfamilies with different subfunctions prior to the last eukaryotic common ancestor.

- The most complex morphological structure of most prokaryotic cells is the flagellum, whose origin seems rooted to structures used in ATP synthase and in secretion systems, with the overall elaborations having arisen in part by gene duplication. Numerous eukaryotes also swim with flagella, but the eukaryotic flagellum evolved independently of that in prokaryotes and operates in a dramatically different way, using cytoskeletal and motor proteins.

- In units of body lengths, swimming rates are several times higher in prokaryotes than eukaryotes, but their operating costs per unit volume are higher as well. The efficiency of conversion of chemical to mechanical energy used in motion is quite low (of order 1%), and as a fraction of a cell's total energy budget, the costs of flagella are on the order of 0.1 to 1.0%, with the costs of construction and operation being of similar magnitudes. Thus, there is a strong selective premium of eliminating flagella unless the advantages outweigh the costs.

Foundations 16.1. The eukaryotic cellular investment in the cytoskeleton. Given the central roles that the cytoskeletal proteins, actin and tubulin, play in eukaryotic cell biology, it is of interest to evaluate the fraction of the cell's energy budget devoted to their production. Estimates are available for the average number of monomers of each protein within the cells of a few species, and this information combined with the cost of protein biosynthesis (to be covered in more detail in Chapter 17) and the cost of building an entire cell (Chapter 8) can be used to obtain a rough estimate of the relative cost of the cytoskeleton.

For the two model yeast species, the average numbers of actin and tubulin monomers per cell are, respectively: 88,600 and 22,400 for *S. cerevisiae* (Norbeck and Blomberg 1997; Kulak et al. 2014); and 731,500 and 125,100 for *S. pombe* (Wu and Pollard 2005; Marguerat et al. 2012; Kulak et al. 2014). Together, these two molecules account for $\sim 0.24\%$ and 0.77% of the total number of proteins per cell in these species.

These numbers can be converted into bioenergetic-cost estimates by noting that: 1) actin and tubulin monomers contain ~ 375 and 450 amino acids, respectively; and 2) the average cost of amino-acid biosynthesis is 30 ATP hydrolyses per amino acid, with another 4 hydrolyses necessary for polypeptide-chain elongation (Chapter 17). Taking the total cost (in ATP hydrolyses per cell cycle) to be the product of the number of monomers, the number of amino acids per monomer, and 34 ATP hydrolyses per amino acid leads to estimates of 1.1×10^9 and 3.3×10^8 for actin and tubulin in *S. cerevisiae,* and 9.1×10^9 and 1.9×10^9 in *S. pombe.* There are additional costs associated with transcription of the genes for these proteins, but as will be more fully discussed in Chapter 17, about 90% of the total cost of running genes is associated with protein production, so the above numbers are only slight underestimates.

To put this into broader perspective, recall that Equation 8.2b provides an estimate of the cost of building an entire cell. Given cell volumes of $\sim 70\,\mu\text{m}^3$ for *S. cerevisiae* and $130\,\mu\text{m}^3$ for *S. pombe,* the number of ATP hydrolyses required for the construction of cells in these two species $\simeq 1.5 \times 10^{12}$ and 2.9×10^{12}, respectively. Thus, just 0.1 and 0.4% of the total energy budgets for cell construction in these species is devoted to the cytoskeleton, with $\sim 80\%$ of such costs being associated with actin. Similar calculations for data from mouse fibroblast cells (Schwanhäusser et al. 2011) leads to estimates of 3.8% for actins and 1.9% for tubulins, and for human HeLa cells (Kulak et al. 2014) of 0.1% for actins and 0.5% for tubulins.

It is of interest to note that the two major cytoskeletal proteins in *E. coli,* FtsZ (related to actin) and MreB (related to tubulin), have average abundances of 3,450 and 1,060 protein monomers per cell (Pla et al. 1991; Rueda et al. 2003; Lu et al. 2007; Taniguchi et al. 2010; Wizniewski and Rakus 2014; Vischer et al. 2015; Ousounov et al. 2016; Bratton et al. 2018), with respective contents of 383 and 347 amino acids/monomer. With the cost of building an *E. coli* cell being $\simeq 27 \times 10^9$ ATP hydrolyses (Chapter 8), the fractional contributions of these two molecules to the total cell budget are 0.16 and 0.04%, respectively. Thus, although the common view is that eukaryotes invest substantially more in cytoskeletal infrastructure than do prokaryotes, this simple comparison suggests just a two-fold increase in yeasts relative to *E. coli.*

Foundations 16.2. The physical challenges to cellular locomotion. A key to understanding the relative advantages / disadvantages of motility in single-celled organisms is the way in which the resistance of a fluid to the motion of an object

scales with the size of the object (Purcell 1977). The central concept is embodied in the definition of a dimensionless index known as the Reynolds number, which equals the ratio of inertial to viscous forces,

$$\mathrm{Re} = \frac{\rho v L}{\eta}, \tag{16.2.1}$$

where ρ is the fluid density (g/cm^3), v is the velocity of the object (cm/sec), L is the characteristic linear dimension of the object (which depends on the shape; cm), and η is the fluid viscosity (g/cm·sec). For water, $\eta/\rho \simeq 10^{-2}$ cm^2/sec. Although the source of Equation 16.2.1 may not be intuitive, the derivation follows from the fact that the inertial force of an object (the numerator in Re) is equal to mass times acceleration (the rate of change of velocity), i.e., $(\rho L^3) \cdot (v/t)$, where t denotes time. The denominator follows from the definition of the coefficient of viscosity (η) as the viscous force per unit area per the velocity gradient (change in velocity per distance), which gives a total viscosity force of $\eta \cdot L^2 \cdot (v/L)$. Noting that $(v/t)/(v/L) = L/t$ is equivalent to v returns $[\,(\rho L^3) \cdot (v/t)\,]/[\,\eta \cdot L^2 \cdot (v/L)\,]$ to Equation 16.2.1.

The Reynolds number is a convenient index of the challenges confronted by an object moving in a fluid. When $\mathrm{Re} < 1$, viscous forces dominate, and in the limiting case of $\mathrm{Re} \ll 1$, the motion at any particular moment is essentially independent of all prior action. In the latter case, the resistance of the fluid is so great that movement of the object ceases nearly instantaneously if the force of motion is stopped. Almost all aspects of cellular movement are in this low Reynolds number range. For example, as noted above for bacterial motility, v is almost always $< 100\,\mu$m/sec, and most bacterial cells have lengths of order $1\,\mu$m, so given that $1\,\mu\mathrm{m} = 10^{-4}$ cm, Re is on the order of 10^{-4}.

A key definition from physics is that power (the rate of doing work, or equivalently the rate of energy utilization) is equal to the product of force and velocity, $P = F \cdot v$. From Stokes' law, which specifically applies to low Reynolds number situations, the inertial drag force is $F = 6\pi r\eta v$, so

$$P = 6\pi r\eta v^2 \tag{16.2.2}$$

for a sphere with radius r. The formula differs for different shapes (see pages 56-57, Berg (1993) for some approximations; and Perrin (1934, 1936) for more general results), although the scaling with ηv^2 remains. One has to be careful with units here. If F in units of kg-m/sec^2, and v has units of m/sec, then P has units of watts or joules/sec. To determine the total metabolic power required to maintain velocity v, the preceding expression must be divided by the efficiency of conversion of electrochemical energy to directional motion (i.e., the ratio of propulsive-power output to rotary-power input), which in *E. coli* is estimated to be 0.017 (Chattopadhyay et al. 2006; and see main text for other estimates).

To determine the potential benefits of swimming in terms of resource acquisition, the overall process can be viewed as being equivalent to a measure of effective diffusion of the cell through the medium. Suppose a cell swims for time τ with constant velocity v in a three-dimensional environment, pauses for infinitesimally short time, and then randomly starts off in a new direction, with the swimming durations being exponentially distributed. Although the physical length of each individual bout is $v\tau$, because the runs are distributed over three dimensions (Chapter 7), and because the times are exponentially distributed, which implies an average squared value of run times of $\overline{\tau^2} = 2\overline{\tau}^2$, the mean-squared length of movement per bout is $2v^2\overline{\tau}^2/3$. By definition, the mean-squared deviation of movement in τ time units is $2D\tau$ (Chapter 7), where D is the diffusion coefficient. Equating these two expressions and factoring out 2τ leads to

$$D = \frac{v^2\tau}{3} \tag{16.2.3a}$$

under the assumption that the directions of movement between adjacent steps are random.

In contrast to the situation in which the directions of successive travel bouts are uncorrelated, if there is some memory of the swimming process such that successive bouts tend to go roughly in the same direction, the average distance traveled is expected to increase. If, however, there is a tendency to switch to opposing directions, the cumulative distance traveled will be decreased. Such correlations of movement can be accommodated by dividing the previous expression by $(1 - \overline{c})$, where $\overline{c}$ is the mean cosine of the angle of switching (Lovely and Dahlquist 1975),

$$D = \frac{v^2 \overline{\tau}}{3(1 - \overline{c})}. \tag{16.2.3b}$$

If the angle of switching is small, $(1 - \overline{c}) \simeq \overline{\theta^2}/2$, where θ is in radians. The mean-squared angular (rotational) deviation $\overline{\theta^2}/2$ is analogous to the mean-squared linear (translational) movement encountered in Chapter 7, leading to the concept of rotational diffusion. By definition then, $\overline{\theta^2}/2 = 2D_r\overline{\tau}$, where D_r is the rotational diffusion coefficient.

Even in the absence of behaviorally-induced switching of angles, the jostling of fluid molecules causes rotational diffusion of the cell, just as in the case of translational movement. It is known that under these conditions $D_r = k_B T/(8\pi\eta r^3)$ (Berg 1993; Equation 6.6). This inverse relationship between the rate of rotational diffusion and cell size means that directional swimming becomes increasingly challenging in small cells that are continually being reoriented by physical forces (Mitchell 1991). Using the preceding approximation for $(1 - \overline{c})$, this leads to an effective diffusion rate of

$$D = \frac{v^2\overline{\tau}}{3(1-\overline{c})} = \frac{2v^2\overline{\tau}}{3\overline{\theta^2}} = \frac{v^2}{6D_r} = \frac{4\pi\eta r^3 v^2}{3k_B T}. \tag{16.2.4a}$$

for a cell at the mercy of random thermal jostling. From Chapter 2, we know that $k_B T \simeq 4.1 \times 10^{-14}$ cm$^2 \cdot$ g $\cdot$ sec^{-2}, and for water $\eta \simeq 10^{-3}$ g $\cdot$ cm$^{-1} \cdot$ sec^{-1}, so for a cell in a freshwater environment, subject to translational and rotational diffusion

$$D \simeq 10^{12} \cdot r^3 v^2, \tag{16.2.4b}$$

where r and v have units of cm and cm/sec, respectively, yielding D with units of cm^2/sec.

If one then considers a bacterium with typical $r \simeq 10^{-4}$ cm, and $v \simeq 3 \times 10^{-3}$ cm/sec, the effective diffusion coefficient is $D \simeq 10^{-5}$ cm^2/sec. From Figure 7.6, the average diffusion coefficient for a typical anion/cation is also $\simeq 10^{-5}$ cm^2/sec, with that for a protein containing 100 amino acids being $\simeq 10^{-6}$ cm^2/sec. The encounter rate between two different types of diffusing particles is proportional to the sum of their diffusion coefficients. Thus, without direct behavioral modifications of swimming direction, a swimming bacterial cell will encounter randomly distributed resources at a rate at least double that expected for a nonmotile cell, and larger, more rapidly swimming cells will achieve more.

An ability to respond to local resource abundance (e.g., by chemotaxis;Chapter 22) can enhance encounter rates by fostering a positive directional bias of movement up a resource gradient. Likewise, a negative bias can lead to local retention in a nutrient-rich patch. Consider, for example, a strong positive correlation of directional movement, $\overline{c} = 0.9$. Applying this to the left-most expression in Equation 16.2.4a, with a bacterial swimming speed of $v \simeq 3\times10^{-3}$ cm/sec and $\overline{\tau} = 1$ sec, leads to $D \simeq 3\times10^{-5}$ cm^2/sec, whereas $\overline{c} = 0$ (random movement) leads to $D \simeq 3 \times 10^{-6}$, and $\overline{c} = -0.8$ leads to $D \simeq 1.7 \times 10^{-6}$ cm^2/sec. Thus, behavioral mechanisms can substantially

magnify average levels of resource availability by biasing movement towards resource-rich patches in a heterogeneous environment.

Arguments like these provide a starting point for estimating costs and benefits of locomotion and chemoreception. Based on a metabolic scaling argument, Dusenbery (1997) estimates that there is a minimal size limit of ~ 0.8 μm below which there is no advantage to motility, although his arguments ignore the cost of building the motility apparatus (Foundations 16.3).

Foundations 16.3. The construction costs of flagella. The cost of building a molecular machine such as a flagellum can be estimated using the general strategy outlined in Foundations 16.1 (with further elaborations on the underpinnings in Chapter 17). For a bacterial flagellum, the biosynthetic costs can be roughly computed as follows. From Berg (2003), an average *E. coli* flagellar filament contains ~ 5340 flagellin protein molecules, each containing ~ 500 amino acids, implying a total investment of $\sim 2.7 \times 10^6$ amino acids/flagellar filament. The remaining proteins associated with the basal body, rod, and hook comprise only about 5% of the protein in the flagellum (Sosinsky et al. 1992; Berg 2003), so in total there are $\sim 3 \times 10^6$ amino acids involved. As noted in Foundations 17.2, the total translation-associated cost per amino acid (including synthesis and polymerization) is ~ 34 ATP hydrolyses, and additional costs of genes at the DNA and mRNA levels only inflate these estimates by $\sim 10\%$. This implies a protein biosynthetic cost per *E. coli* flagellum of $\sim 10^8$ ATP hydrolyses.

For some bacteria, there is an additional cost of wrapping the filament with a lipid membrane. Although not one of these, *E. coli* will nonetheless be used here to examine the consequences of such an elaboration. Again, the details underlying the computations will be given in Chapter 17. The essential points are that with an average *E. coli* flagellum radius and length of 0.01 and 6 μm, respectively, the cylindrical surface area of the flagellum is $\sim 0.4\,\mu\text{m}^2$. As the average membrane area occupied by a bacterial lipid molecule is $0.65 \times 10^{-6}\,\mu\text{m}^2$, after accounting for the two leaflets of the lipid bilayer, there would be an estimated 1.2×10^6 lipid molecules surrounding this flagellum. The biosynthetic costs of lipids are much greater than those for proteins, averaging 300 ATP hydrolyses per lipid molecule, leading to a total biosynthetic cost of the flagellar membrane of $\sim 3.6 \times 10^8$ ATP hydrolyses, $\sim 4\times$ that of the protein components.

To extend these calculations to eukaryotes, consider the green alga *Chlamydomonas reinhardtii,* which generally has two flagella with approximate radii and lengths of 0.075 and 20 μm. After accounting for the slightly elevated cost of lipid biosynthesis in eukaryotes ($\simeq 350$ ATPs), this implies a total membrane cost surrounding each flagellum of $\sim 10^{10}$ ATP. Raven and Richardson (1984) estimate there to be $\sim 48,000$ tubulin monomers (each ~ 450 amino acids in length) per μm of flagellum, implying a cost for this major molecule of $\sim 1.5 \times 10^{10}$ ATP. There are also ~ 600 of the large motor protein dynein (each $\sim 15,000$ amino acids in length) per μm, implying an additional construction cost of $\sim 6.1 \times 10^9$ ATP. There are numerous other proteins within eukaryotic flagella, including the smaller motor protein kinesin, but their summed number is unlikely to rival that for tubulin and dynein, so the total cost of protein synthesis associated with each *C. reinhardtii* flagellum is $\sim 3 \times 10^{10}$ ATP. This is $\sim 3\times$ the lipid cost, opposite the situation for a bacterial flagellum, but expectedly so, given the lower surface area:volume ratio of the thicker eukaryotic flagellum.

Literature Cited

Akhmanova, A., and M. O. Steinmetz. 2015. Control of microtubule organization and dynamics: two ends in the limelight. Nat. Rev. Mol. Cell. Biol. 16: 711-726.

Albers, S. V., and K. F. Jarrell. 2018. The archaellum: an update on the unique archaeal motility structure. Trends Microbiol. 26: 351-362.

Albers, S. V., and B. H. Meyer. 2011. The archaeal cell envelope. Nat. Rev. Microbiol. 9: 414-426.

Albers, S. V., and M. Pohlschröder. 2009. Diversity of archaeal type IV pilin-like structures. Extremophiles 13: 403-410.

Alliegro, M. C., and P. Satir. 2009. Origin of the cilium: novel approaches to examine a centriolar evolution hypothesis. Methods Cell Biol. 94: 53-64.

Amir, A., F. Babaeipour, D. B. McIntosh, D. R. Nelson, and S. Jun. 2014. Bending forces plastically deform growing bacterial cell walls. Proc. Natl. Acad. Sci. USA 111: 5778-5783.

Arroyo, M., L. Heltai, D. Millán, and A. DeSimone. 2012. Reverse engineering the euglenoid movement. Proc. Natl. Acad. Sci. USA 109: 17874-17879.

Asmar, A. T., and J. F. Collet. 2018. Lpp, the Braun lipoprotein, turns 50-major achievements and remaining issues. FEMS Microbiol. Lett. 365 (18).

Avidor-Reiss, T., A. M. Maer, E. Koundakjian, A. Polyanovsky, T. Keil, S. Subramaniam, and C. S. Zuker. 2004. Decoding cilia function: defining specialized genes required for compartmentalized cilia biogenesis. Cell 117: 527-539.

Barsanti, L., P. Coltelli, V. Evangelista, A. M. Frassanito, and P. Gualtieri. 2016. Swimming patterns of the quadriflagellate *Tetraflagellochloris mauritanica* (Chlamydomonadales, Chlorophyceae). J. Phycol. 52: 209-218.

Bazylinski, D. A., R. B. Frankel. 2004. Magnetosome formation in prokaryotes. Nat. Rev. Microbiol. 2: 217-230.

Becker, B. 2000. The cell surface of flagellates, pages 110-123. In B. S. C. Leadbeater and J. C. G. Taylor (eds.) The Flagellates: Unity, Diversity, and Evolution. Taylor and Francis, New York, NY.

Berg, H. C. 1993. Random Walks in Biology. Princeton Univ. Press, Princeton, NJ.

Berg, H. C. 2003. The rotary motor of bacterial flagella. Annu. Rev. Biochem. 72: 19-54.

Bernander, R., and T. J. Ettema. 2010. FtsZ-less cell division in archaea and bacteria. Curr. Opin. Microbiol. 13: 747-752.

Billaudeau, C., A. Chastanet, Z. Yao, C. Cornilleau, N. Mirouze, V. Fromion, and R. Carballido-López. 2017. Contrasting mechanisms of growth in two model rod-shaped bacteria. Nat. Commun. 8: 15370.

Block, S. M., L. S. Goldstein, and B. J. Schnapp. 1990. Bead movement by single kinesin molecules studied with optical tweezers. Nature 348: 348-352.

Blocker, A., K. Komoriya, and S. Aizawa. 2003. Type III secretion systems and bacterial flagella: insights into their function from structural similarities. Proc. Natl. Acad. Sci. USA 100: 3027-3030.

Boehm, A., M. Kaiser, H. Li, C. Spangler, C. A. Kasper, M. Ackermann, V. Kaever, V. Sourjik, V. Roth, and U. Jenal. 2010. Second messenger-mediated adjustment of bacterial swimming velocity. Cell 141: 107-116.

Bratton, B. P., J. W. Shaevitz, Z. Gitai, and R. M. Morgenstein. 2018. MreB polymers and curvature localization are enhanced by RodZ and predict *E. coli*'s cylindrical uniformity. Nat. Commun. 9: 2797.

Braun, T., A. Orlova, K. Valegård, A. C. Lindås, G. F. Schröder, and E. H. Egelman. 2015. Archaeal actin from a hyperthermophile forms a single-stranded filament. Proc. Natl. Acad. Sci. USA 112: 9340-9345.

Brunet, T., M. Albert, W. Roman, M. C. Coyle MC, D. C. Spitzer, and N. King. 2021. A flagellate-to-amoeboid switch in the closest living relatives of animals. eLife 10: e61037.

Carlier, M. F., and S. Shekhar. 2017. Global treadmilling coordinates actin turnover and controls the size of actin networks. Nat. Rev. Mol. Cell. Biol. 18: 389-401.

Carvalho-Santos, Z., J. Azimzadeh, J. B. Pereira-Leal, and M. Bettencourt-Dias. 2011. Evolution: tracing the origins of centrioles, cilia, and flagella. J. Cell Biol. 194: 165-175.

Carvalho-Santos, Z., P. Machado, P. Branco, F. Tavares-Cadete, A. Rodrigues-Martins, J. B. Pereira-Leal, and M. Bettencourt-Dias. 2010. Stepwise evolution of the centriole-assembly pathway. J. Cell Sci. 123: 1414-1426.

Cavalier-Smith, T. 1978. The evolutionary origin and phylogeny of microtubules, mitotic spindles and eukaryote flagella. Biosystems 10: 93-114.

Cavalier-Smith, T. 2002. The phagotrophic origin of eukaryotes and phylogenetic classification of Protozoa. Internat. J. Syst. Evol. Microbiol. 52: 297-354.

Chaban, B., I. Coleman, and M. Beeby. 2018. Evolution of higher torque in *Campylobacter*-type bacterial flagellar motors. Sci. Rep. 8: 97.

Chattopadhyay, S., R. Moldovan, C. Yeung, and X. L. Wu. 2006. Swimming efficiency of bacterium *Escherichia coli*. Proc. Natl. Acad. Sci. USA 103: 13712-13717.

Chen, S., et al. 2011. Structural diversity of bacterial flagellar motors. EMBO J. 30: 2972-2981.

Chia, F.-S., J. Buckland-Nicks, and C. M. Young. 1984. Locomotion of marine invertebrate larvae: a review. Can. J. Zool. 62: 1205-1222.

Cochran, J. C. 2015. Kinesin motor enzymology: chemistry, structure, and physics of nanoscale molecular machines. Biophys. Rev. 7: 269-299.

Crawford, D. W. 1992. Metabolic cost of motility in planktonic protists: theoretical considerations on size scaling and swimming speed. Microb. Ecol. 24: 1-10.

Daum, B., J. Vonck, A. Bellack, P. Chaudhury, R. Reichelt, S. V. Albers, R. Rachel, and W. Kühlbrandt. 2017. Structure and *in situ* organisation of the *Pyrococcus furiosus* archaellum machinery. Elife 6: e27470.

Deng, X., G. Fink, T. A. M. Bharat, S. He, D. Kureisaite-Ciziene, and J. Löwe. 2017. Four-stranded mini microtubules formed by *Prosthecobacter* BtubAB show dynamic instability. Proc. Natl. Acad. Sci. USA 114: E5950-E5958.

Desmond, E., C. Brochier-Armanet, and S. Gribaldo. 2007. Phylogenomics of the archaeal flagel-

lum: rare horizontal gene transfer in a unique motility structure. BMC Evol. Biol. 7: 106.

Dishinger, J. F., H. L. Kee, P. M. Jenkins, S. Fan, T. W. Hurd, J. W. Hammond, Y. N. Truong, B. Margolis, J. R. Martens, and K. J. Verhey. 2010. Ciliary entry of the kinesin-2 motor KIF17 is regulated by importin-beta2 and RanGTP. Nat. Cell Biol. 12: 703-710.

Domozych, D. S., et al. 2014. Pectin metabolism and assembly in the cell wall of the charophyte green alga *Penium margaritaceum.* Plant Physiol. 165: 105-118.

Dusenbery, D. B. 1997. Minimum size limit for useful locomotion by free-swimming microbes. Proc. Natl. Acad. Sci. USA 94: 10949-10954.

Dusenbery, D. B. 1998. Fitness landscapes for effects of shape on chemotaxis and other behaviors of bacteria. J. Bacteriol. 180: 5978-5983.

Dutcher, S. K. 2003. Long-lost relatives reappear: identification of new members of the tubulin superfamily. Curr. Opin. Microbiol. 6: 634-640.

Egelman, E. H. 2010. Reducing irreducible complexity: divergence of quaternary structure and function in macromolecular assemblies. Curr. Opin. Cell Biol. 22: 68-74.

Elting, M. W., Z. Bryant, J. C. Liao, and J. A. Spudich. 2011. Detailed tuning of structure and intramolecular communication are dispensable for processive motion of myosin VI. Biophys. J. 100: 430-439.

Erickson, H. P. 2007. Evolution of the cytoskeleton. Bioessays 29: 668-677.

Ettema, T. J., A. C. Lindås, and R. Bernander. 2011. An actin-based cytoskeleton in archaea. Mol. Microbiol. 80: 1052-1061.

Fai, T. G., L. Mohapatra, P. Kar, J. Kondev, and A. Amir. 2019. Length regulation of multiple flagella that self-assemble from a shared pool of components. eLife 8: e42599.

Fenchel, T., and B. J. Finlay. 1983. Respiration rates in heterotrophic, free-living protozoa. Microb. Ecol. 9: 99122.

Ferreira, J. L., et al. 2019. γ-proteobacteria eject their polar flagella under nutrient depletion, retaining flagellar motor relic structures. PLoS Biol. 17: e3000165.

Flamholz, A., R. Phillips, and R. Milo. 2014. The quantified cell. Mol. Biol. Cell 25: 3497-3500.

Foth, B. J., M. C. Goedecke, and D. Soldati. 2006. New insights into myosin evolution and classification. Proc. Natl. Acad. Sci. USA 103: 3681-3686.

Fritz-Laylin, L. K., S. J. Lord, and R. D. Mullins. 2017. WASP and SCAR are evolutionarily conserved in actin-filled pseudopod-based motility. J. Cell Biol. 216: 1673-1688.

Fulton, C. 1977. Cell differentiation in *Naegleria gruberi.* Annu. Rev. Microbiol. 31: 597-629.

Galkin, V. E., X. Yu, J. Bielnicki, J. Heuser, C. P. Ewing, P. Guerry, and E. H. Egelman. 2008. Divergence of quaternary structures among bacterial flagellar filaments. Science 320: 382-385.

Gardner, M. K., M. Zanic, and J. Howard. 2013. Microtubule catastrophe and rescue. Curr. Opin. Cell. Biol. 25: 14-22.

Geis, G, Suerbaum S, Forsthoff B, Leying H, and Opferkuch W. 1993. Ultrastructure and biochemical studies of the flagellar sheath of *Helicobacter pylori.* J. Med. Microbiol. 38: 371-377.

Ghoshdastider, U., S. Jiang, D. Popp, and R. C. Robinson. 2015. In search of the primordial actin

filament. Proc. Natl. Acad. Sci. USA 112: 9150-9151.

Gilbert, J. J. 1994. Jumping behavior in the oligotrich ciliates *Strobilidium velox* and *Halteria grandinella,* and its significance as a defense against rotifer predators. Microb. Ecol. 27: 189-200.

Ginger, M. L., N. Portman, and P. G. McKean. 2008. Swimming with protists: perception, motility and flagellum assembly. Nat. Rev. Microbiol. 6: 838-850.

Gittleson, S. M., and R. M. Noble. 1973. Locomotion in *Polytomella agilis* and *Polytoma uvella.* Trans. Amer. Micro. Soc. 92: 122-128

Gönczy, P. 2012. Towards a molecular architecture of centriole assembly. Nat. Rev. Mol. Cell Biol. 13: 425-435.

Goodson, H. V., and S. C. Dawson. 2006. Multiplying myosins. Proc. Natl. Acad. Sci. USA 103: 3498-3499.

Goodson, H. V., and W. F. Hawse. 2002. Molecular evolution of the actin family. J. Cell Sci. 115: 2619-2622.

Gumbart, J. C., M. Beeby, G. J. Jensen, and B. Roux. 2014. *Escherichia coli* peptidoglycan structure and mechanics as predicted by atomic-scale simulations. PLoS Comput. Biol. 10: e1003475.

Hariharan, V., and W. O. Hancock. 2009. Insights into the mechanical properties of the kinesin neck linker domain from sequence analysis and molecular dynamics simulations. Cell. Mol. Bioeng. 2: 177189.

Hartman, H., and T. F. Smith. 2009. The evolution of the cilium and the eukaryotic cell. Cell Motil. Cytoskeleton 66: 215-219.

Hartmann, E., and H. König. 1990. Comparison of the biosynthesis of the methanobacterial pseudomurein and the eubacterial murein. Naturwissenschaften 77: 472-475.

Hodges, M. E., N. Scheumann, B. Wickstead, J. A. Langdale, and K. Gull. 2010. Reconstructing the evolutionary history of the centriole from protein components. J. Cell Sci. 123: 1407-1413.

Horio, T., and B. R. Oakley. 1994. Human gamma-tubulin functions in fission yeast. J. Cell. Biol. 126: 1465-1473.

Hou, Y., R. Sierra, D. Bassen, N. K. Banavali, A. Habura, J. Pawlowski, and S. S. Bowser. 2013. Molecular evidence for β-tubulin neofunctionalization in Retaria (Foraminifera and radiolarians). Mol. Biol. Evol. 30: 2487-2493.

Howard, J. 2001. Mechanics of Motor Proteins and the Cytoskeleton. Sinauer Assocs., Inc. Sunderland, MA.

Hwang, W., and Karplus M. 2019. Structural basis for power stroke vs. Brownian ratchet mechanisms of motor proteins. Proc. Natl. Acad. Sci. USA 116: 19777-19785.

Ishikawa, H., and W. F. Marshall. 2011. Ciliogenesis: building the cell's antenna. Nat. Rev. Mol. Cell Biol. 12: 222-234.

Ishikawa, H., and W. F. Marshall. 2017. Testing the time-of-flight model for flagellar length sensing. Mol. Biol. Cell. 28: 3447-3456.

Ito, M., and Y. Takahashi. 2017. Nonconventional cation-coupled flagellar motors derived from the

alkaliphilic *Bacillus* and *Paenibacillus* species. Extremophiles 21: 3-14.

Izoré, T., D. Kureisaite-Ciziene, S. H. McLaughlin, and J. Löwe. 2016. Crenactin forms actin-like double helical filaments regulated by arcadin-2. eLife 5: e21600.

Jarrell, K. F., and M. J. McBride. 2008. The surprisingly diverse ways that prokaryotes move. Nat. Rev. Microbiol. 6: 466-476.

Jékely, G., and D. Arendt. 2006. Evolution of intraflagellar transport from coated vesicles and autogenous origin of the eukaryotic cilium. Bioessays 28: 191-198.

Joseph, J. M., P. Fey, N. Ramalingam, X. I. Liu, M. Rohlfs, A. A. Noegel, A. Müller-Taubenberger, G. Glöckner, and M. Schleicher. 2008. The actinome of *Dictyostelium discoideum* in comparison to actins and actin-related proteins from other organisms. PLoS One 3: e2654.

Kaplan, M., D. Ghosal, P. Subramanian, C. M. Oikonomou, A. Kjaer, S. Pirbadian, D. R. Ortega, A. Briegel, M. Y. El-Naggar, and G. J. Jensen. 2019. The presence and absence of periplasmic rings in bacterial flagellar motors correlates with stator type. eLife 8: e43487.

Kardon, J. R., and R. D. Vale. 2009. Regulators of the cytoplasmic dynein motor. Nat. Rev. Mol. Cell. Biol. 10: 854-865.

Katsu-Kimura, Y., F. Nakaya, S. A. Baba, and Y. Mogami. 2009. Substantial energy expenditure for locomotion in ciliates verified by means of simultaneous measurement of oxygen consumption rate and swimming speed. J. Exp. Biol. 212: 1819-1824.

Kee, H. L., J. F. Dishinger, T. L. Blasius, C. J. Liu, B. Margolis, and K. J. Verhey. 2012. A size-exclusion permeability barrier and nucleoporins characterize a ciliary pore complex that regulates transport into cilia. Nat. Cell Biol. 14: 431-437.

Khona, D. K., et al. 2013. Anomalies in the motion dynamics of long-flagella mutants of *Chlamydomonas reinhardtii.* J. Biol. Phys. 39: 1-14.

Kiefel, B. R., P. R. Gilson, and P. L. Beech. 2004. Diverse eukaryotes have retained mitochondrial homologues of the bacterial division protein FtsZ. Protist 155: 105-115.

Kinosita, Y., N. Uchida, D. Nakane, and T. Nishizaka. 2016. Direct observation of rotation and steps of the archaellum in the swimming halophilic archaeon *Halobacterium salinarum.* Nat. Microbiol. 1: 16148.

Klis, F. M., C. G. de Koster, and S. Brul. 2014. Cell wall-related bionumbers and bioestimates of *Saccharomyces cerevisiae* and *Candida albicans.* Eukaryot. Cell 13: 2-9.

Kollmar, M., D. Lbik, and S. Enge. 2012. Evolution of the eukaryotic ARP2/3 activators of the WASP family WASP, WAVE, WASH, and WHAMM, and the proposed new family members WAWH and WAML. BMC Res. Notes 5: 88.

Kulak, N. A., G. Pichler, I. Paron, N. Nagaraj, and M. Mann. 2014. Minimal, encapsulated proteomic-sample processing applied to copy-number estimation in eukaryotic cells. Nat. Methods 11: 319-324.

Kull, F. J., R. D. Vale, and R. J. Fletterick. 1998. The case for a common ancestor: kinesin and myosin motor proteins and G proteins. J. Muscle Res. Cell Motil. 19: 877-886.

Larsen, R. A., C. Cusumano, A. Fujioka, G. Lim-Fong, P. Patterson, and J. Pogliano. 2007. Treadmilling of a prokaryotic tubulin-like protein, TubZ, required for plasmid stability in *Bacillus thuringiensis.* Genes Dev. 21: 1340-1352.

Lassak, K., T. Neiner, A. Ghosh, A. Klingl, R. Wirth, and S. V. Albers. 2012. Molecular analysis of the crenarchaeal flagellum. Mol. Microbiol. 83: 110-124.

Lawrence, C. J., et al.. 2004. A standardized kinesin nomenclature. J. Cell Biol. 167: 19-22.

Li, G. W., D. Burkhardt, C. Gross, and J. S. Weissman. 2014. Quantifying absolute protein synthesis rates reveals principles underlying allocation of cellular resources. Cell 157: 624635.

Lindås, A. C., E. A. Karlsson, M. T. Lindgren, T. J. Ettema, and R. Bernander. 2008. A unique cell division machinery in the Archaea. Proc. Natl. Acad. Sci. USA 105: 18942-18946.

Liu, R., and H. Ochman. 2007. Stepwise formation of the bacterial flagellar system. Proc. Natl. Acad. Sci. USA 104: 7116-7121.

Lleo, M. M., P. Canepari, and G. Satta. 1990. Bacterial cell shape regulation: testing of additional predictions unique to the two-competing-sites model for peptidoglycan assembly and isolation of conditional rod-shaped mutants from some wild-type cocci. J. Bacteriol. 172: 3758-3771.

Lovely, P. S., and F. W. Dahlquist. 1975. Statistical measures of bacterial motility and chemotaxis. J. Theor. Biol. 50: 477-496.

Löwe, J., and L. A. Amos. 2009. Evolution of cytomotive filaments: the cytoskeleton from prokaryotes to eukaryotes. Int. J. Biochem. Cell Biol. 41: 323-329.

Lu, P., C. Vogel, R. Wang, X. Yao, and E. M. Marcotte. 2007. Absolute protein expression profiling estimates the relative contributions of transcriptional and translational regulation. Nat. Biotechnol. 25: 117-124.

Ludington, W. B., L. Z. Shi, Q. Zhu, M. W. Berns, and W. F. Marshall. 2012. Organelle size equalization by a constitutive process. Curr. Biol. 22: 2173-2179.

Ludington, W. B., K. A. Wemmer, K. F. Lechtreck, G. B. Witman, and W. F. Marshall. 2013. Avalanche-like behavior in ciliary import. Proc. Natl. Acad. Sci. USA 110: 3925-30.

Lynch, M., and G. K. Marinov. 2015. The bioenergetic costs of a gene. Proc. Natl. Acad. Sci. USA 112: 15690-15695.

Lynch, M., and B. Trickovic. 2020. A theoretical framework for evolutionary cell biology. J. Mol. Biol. 432: 1861-1879.

Maezawa, K., S. Shigenobu, H. Taniguchi, T. Kubo, S. Aizawa, and M. Morioka. 2006. Hundreds of flagellar basal bodies cover the cell surface of the endosymbiotic bacterium *Buchnera aphidicola* sp. strain APS. J. Bacteriol. 188: 6539-6543.

Makarova, K. S., N. Yutin, S. D. Bell, and E. V. Koonin. 2010. Evolution of diverse cell division and vesicle formation systems in Archaea. Nat. Rev. Microbiol. 8: 731-741.

Männik, J., R. Driessen, P. Galajda, J. E. Keymer, and C. Dekker. 2009. Bacterial growth and motility in sub-micron constrictions. Proc. Natl. Acad. Sci. USA 106: 14861-14866.

Manson, M. D., P. M. Tedesco, and H. C. Berg. 1980. Energetics of flagellar rotation in bacteria. J. Mol. Biol. 138: 541-561.

Manson, M. D., P. Tedesco, H. C. Berg, F. M. Harold, and C. Van der Drift. 1977. A proton motive force drives bacterial flagella. Proc. Natl. Acad. Sci. USA 74: 3060-3064.

Margolin, W. 2009. Sculpting the bacterial cell. Curr. Biol. 19: R812-R822.

Marguerat, S., A. Schmidt, S. Codlin, W. Chen, R. Aebersold, and J. Bähler. 2012. Quantitative analysis of fission yeast transcriptomes and proteomes in proliferating and quiescent cells. Cell 151: 671-683.

Marshall, W. F. 2011. Origins of cellular geometry. BMC Biol. 9: 57.

Marshall, W. F., and J. L. Rosenbaum. 2001. Intraflagellar transport balances continuous turnover of outer doublet microtubules: implications for flagellar length control. J. Cell Biol. 155: 405-414.

Mast, F. D., R. A. Rachubinski, and J. B. Dacks. 2012. Emergent complexity in myosin V-based organelle inheritance. Mol. Biol. Evol. 29: 975-984.

McInally, S. G., J. Kondev, and S. C. Dawson. 2019. Length-dependent disassembly maintains four different flagellar lengths in *Giardia*. eLife 8: e48694.

McKean, P. G., S. Vaughan, and K. Gull. 2001. The extended tubulin superfamily. J. Cell Sci. 114: 2723-2733.

Meister, M., G. Lowe, and H. C. Berg. 1987. The proton flux through the bacterial flagellar motor. Cell 49: 643-650.

Michel, G., T. Tonon, D. Scornet, J. M. Cock, and B. Kloareg. 2010. The cell wall polysaccharide metabolism of the brown alga *Ectocarpus siliculosus*. Insights into the evolution of extracellular matrix polysaccharides in Eukaryotes. New Phytol. 188: 82-97.

Michie, K. A., and J. Löwe. 2006. Dynamic filaments of the bacterial cytoskeleton. Annu. Rev. Biochem. 75: 467-492.

Mitchell, J. G. 1991. The influence of cell size on marine bacterial motility and energetics. Microbial Ecol. 22: 227-238.

Monds, R. D., T. K. Lee, A. Colavin, T. Ursell, S. Quan, T. F. Cooper, and K. C. Huang. 2014. Systematic perturbation of cytoskeletal function reveals a linear scaling relationship between cell geometry and fitness. Cell Rep. 9: 1528-1537.

Moon, K. H., X. Zhao, A. Manne, J. Wang, Z. Yu, J. Liu, and M. A. Motaleb. 2016. Spirochetes flagellar collar protein FlbB has astounding effects in orientation of periplasmic flagella, bacterial shape, motility, and assembly of motors in *Borrelia burgdorferi*. Mol. Microbiol. 102: 336-348.

Muthukrishnan, G., Y. Zhang, S. Shastry, and W. O. Hancock. 2009. The processivity of kinesin-2 motors suggests diminished front-head gating. Curr. Biol. 19: 442-447.

Nan, B., and D. R. Zusman. 2016. Novel mechanisms power bacterial gliding motility. Mol. Microbiol. 101: 186-193.

Neidhardt, F. C., J. L. Ingraham, and M. Schaechter. 1990. Physiology of the bacterial cell: a molecular approach. Sinauer Assoc., Inc., Sunderland, MA.

Nevers, Y., et al. 2017. Insights into ciliary genes and evolution from multi-level phylogenetic profiling. Mol. Biol. Evol. 34: 2016-2034.

Niklas, K. J. 2004. The cell walls that bind the Tree of Life. BioScience 54: 831-841.

Norbeck, J., and A. Blomberg. 1997. Two-dimensional electrophoretic separation of yeast proteins using a non-linear wide range (pH 3-10) immobilized pH gradient in the first dimension; reproducibility and evidence for isoelectric focusing of alkaline (pI $>$ 7) proteins. Yeast 13:

1519-1534.

Oger, P. M., and A. Cario. 2013. Adaptation of the membrane in Archaea. Biophys. Chem. 183: 42-56.

Ojkic, N., D. Serbanescu, and S. Banerjee. 2019. Surface-to-volume scaling and aspect ratio preservation in rod-shaped bacteria. eLife 8: e47033.

Okuda, K. 2002. Structure and phylogeny of cell coverings. J. Plant Res. 115: 283-288.

Osawa, M., and H. P. Erickson. 2006. FtsZ from divergent foreign bacteria can function for cell division in *Escherichia coli*. J. Bacteriol. 188: 7132-7140.

Ouzounov, N., J. P. Nguyen, B. P. Bratton, D. Jacobowitz, Z. Gitai, and J. W. Shaevitz. 2016. MreB orientation correlates with cell diameter in *Escherichia coli*. Biophys. J. 111: 1035-1043.

Ozyamak, E., J. M. Kollman, and A. Komeili. 2013. Bacterial actins and their diversity. Biochemistry 52: 6928-6939.

Pallen, M. J., and N. J. Matzke. 2006. From The Origin of Species to the origin of bacterial flagella. Nat. Rev. Microbiol. 4: 784-790.

Pallen, M. J., C. W. Penn, and R. R. Chaudhuri. 2005. Bacterial flagellar diversity in the post-genomic era. Trends Microbiol. 13: 143-149.

Pančić, M., R. R. Torres, R. Almeda, and T. Kiørboe. 2019. Silicified cell walls as a defensive trait in diatoms. Proc. Biol. Sci. 286: 20190184.

Pazour, G. J., N. Agrin, J. Leszyk, and G. B. Witman. 2005. Proteomic analysis of a eukaryotic cilium. J. Cell. Biol. 170: 103-113.

Pelve, E. A., A. C. Lindås, W. Martens-Habbena, J. R. de la Torre, D. A. Stahl, and R. Bernander. 2011. Cdv-based cell division and cell cycle organization in the thaumarchaeon *Nitrosopumilus maritimus*. Mol. Microbiol. 82: 555-566.

Pérez-Núñez, D., R. Briandet, B. David, C. Gautier, P. Renault, B. Hallet, P. Hols, R. Carballido-López, and E. Guédon. 2011. A new morphogenesis pathway in bacteria: unbalanced activity of cell wall synthesis machineries leads to coccus-to-rod transition and filamentation in ovococci. Mol. Microbiol. 79: 759-771.

Perrin, F. 1934. Mouvement Brownien d'un ellipsoide. I. Dispersion dilectrique pour des molécules ellipsoidales. J. Phys. Radium 5: 497-511.

Perrin, F. 1936. Mouvement Brownien d'un ellipsoide. II. Rotation libre et dépolarisation des fluorescences. Translation et diffusion de molécules ellipsoidales. J. Phys. Radium 7: 1-11.

Pilhofer, M., M. S. Ladinsky, A. W. McDowall, G. Petroni, and G. J. Jensen. 2011. Microtubules in bacteria: ancient tubulins build a five-protofilament homolog of the eukaryotic cytoskeleton. PLoS Biol. 9: e1001213.

Pla, J., M. Sanchez, P. Palacios, M. Vicente, and M. Aldea. 1991. Preferential cytoplasmic location of FtsZ, a protein essential for *Escherichia coli* septation. Mol. Microbiol. 5: 1681-1686.

Preisner, H., J. Habicht, S. G. Garg, and S. B. Gould. 2018. Intermediate filament protein evolution and protists. Cytoskeleton 75: 231-243.

Preston, T. M., and C. A. King. 2003. Locomotion and phenotypic transformation of the amoeboflagellate *Naegleria gruberi* at the water-air interface. J. Eukaryot. Microbiol. 50: 245-251.

Prostak, S. M., K. A. Robinson, M. A. Titus, and L. K. Fritz-Laylin. 2021. The actin networks of chytrid fungi reveal evolutionary loss of cytoskeletal complexity in the fungal kingdom. Curr. Biol. 31: 1192-1205.

Purcell, E. M. 1977. Life at low Reynolds number. Amer. J. Physics 45: 3-11.

Quintero, O. A., and C. M. Yengo. 2012. Myosin X dimerization and its impact on cellular functions. Proc. Natl. Acad. Sci. USA 109: 17313-17314.

Raven, J. A. 1982. The energetics of freshwater algae; energy requirements for biosynthesis and volume regulation. New Phytol. 92: 1-20.

Raven, J. A. 1983. The transport and function of silicon in plants. Biol. Rev. 58: 179-207.

Raven, J. A., and K. Richardson. 1984. Dinophyte flagella: a cost-benefit analysis. New Phytol. 98: 259-276

Richards, T. A., and T. Cavalier-Smith. 2005. Myosin domain evolution and the primary divergence of eukaryotes. Nature 436: 1113-1118.

Richards, T. A., et al. 2004. A standardized kinesin nomenclature. J. Cell Biol. 167: 19-22.

Rosenbaum, J. L., and G. B. Witman. 2002. Intraflagellar transport. Nat. Rev. Mol. Cell Biol. 3: 813-825.

Rossmann, F. M., and M. Beeby. 2018. Insights into the evolution of bacterial flagellar motors from high-throughput *in situ* electron cryotomography and subtomogram averaging. Acta Crystallogr. D Struct. Biol. 74: 585-594.

Rueda, S., M. Vicente, and J. Mingorance. 2003. Concentration and assembly of the division ring proteins FtsZ, FtsA, and ZipA during the *Escherichia coli* cell cycle. J. Bacteriol. 185: 3344-3351.

Salje, J., P. Gayathri, and J. Löwe. 2010. The ParMRC system: molecular mechanisms of plasmid segregation by actin-like filaments. Nat. Rev. Microbiol. 8: 683-692.

Samson, R. Y., and S. D. Bell. 2009. Ancient ESCRTs and the evolution of binary fission. Trends Microbiol. 17: 507-513.

Satir, P., C. Guerra, and A. J. Bell. 2007. Evolution and persistence of the cilium. Cell Motil. Cytoskeleton 64: 906-913.

Sato, K., et al. 2007. Stroke frequency, but not swimming speed, is related to body size in free-ranging seabirds, pinnipeds and cetaceans. Proc. Biol. Sci. 274: 471-477.

Saxena, I. M., R. M. Brown, Jr. 2005. Cellulose biosynthesis: current views and evolving concepts. Ann. Bot. 96: 9-21.

Scholey, J. M. 2013. Kinesin-2: a family of heterotrimeric and homodimeric motors with diverse intracellular transport functions. Annu. Rev. Cell Dev. Biol. 29: 443-469.

Schwanhäusser, B., D. Busse, N. Li, G. Dittmar, J. Schuchhardt, J. Wolf, W. Chen, and M. Selbach. 2011. Global quantification of mammalian gene expression control. Nature 473: 337-342.

Sehring, I. M., C. Reiner, J. Mansfeld, H. Plattner, and R. Kissmehl. 2007. A broad spectrum of actin paralogs in *Paramecium tetraurelia* cells display differential localization and function. J. Cell Sci. 120: 177-190.

Seidler, R. J., and M. P. Starr. 1968. Structure of the flagellum of *Bdellovibrio bacteriovorus.* J. Bacteriol. 95: 1952-1955.

Shastry, S., and W. O. Hancock. 2010. Neck linker length determines the degree of processivity in kinesin-1 and kinesin-2 motors. Curr. Biol. 20: 939-943.

Siefert, J. L., and G. E. Fox. 1998. Phylogenetic mapping of bacterial morphology. Microbiology 144: 2803-2808.

Smith, J. C., J. G. Northey, J. Garg, R. E. Pearlman, and K. W. Siu. 2005. Robust method for proteome analysis by MS/MS using an entire translated genome: demonstration on the ciliome of *Tetrahymena thermophila.* J. Proteome Res. 4: 909-919.

Sosinsky, G. E., N. R. Francis, D. J. DeRosier, J. S. Wall, M. N. Simon, and J. Hainfeld. 1992. Mass determination and estimation of subunit stoichiometry of the bacterial hook-basal body flagellar complex of *Salmonella typhimurium* by scanning transmission electron microscopy. Proc. Natl. Acad. Sci. USA 89: 4801-4805.

Steenbakkers, P. J., W. J. Geerts, N. A. Ayman-Oz, and J. T. Keltjens. 2006. Identification of pseudomurein cell wall binding domains. Mol. Microbiol. 62: 1618-1630.

Stepanek, L., and G. Pigino. 2016. Microtubule doublets are double-track railways for intraflagellar transport trains. Science 352: 721-724.

Snyder, L. A., N. J. Loman, K. Fütterer, and M. J. Pallen. 2009. Bacterial flagellar diversity and evolution: seek simplicity and distrust it? Trends Microbiol. 17: 1-5.

Sweeney, H. L., and E. L. F. Holzbaur. 2016. Motor proteins, Pages 69-86. In T. D. Pollard and R. D. Goldman (eds.) The Cytoskeleton. Cold Spring Harbor Laboratory Press, Cold Spring Harbor, NY.

Szewczak-Harris, A., and J. Löwe. 2018. Cryo-EM reconstruction of AlfA from *Bacillus subtilis* reveals the structure of a simplified actin-like filament at 3.4-Åresolution. Proc. Natl. Acad. Sci. USA 115: 3458-3463.

Tam, L. W., W. L. Dentler, and P. A. Lefebvre. 2003. Defective flagellar assembly and length regulation in LF3 null mutants in *Chlamydomonas.* J. Cell Biol. 163: 597-607.

Tam, D., and A. E. Hosoi. 2011. Optimal feeding and swimming gaits of biflagellated organisms. Proc. Natl. Acad. Sci. USA 108: 1001-1006.

Tamames, J., M. Gonzalez-Moreno, J. Mingorance, A. Valencia, and M. Vicente. 2001. Bringing gene order into bacterial shape. Trends Genet. 17: 124-126.

Taniguchi, Y., P. J. Choi, G. W. Li, H. Chen, M. Babu, J. Hearn, A. Emili, and X. S. Xie. 2010. Quantifying *E. coli* proteome and transcriptome with single-molecule sensitivity in single cells. Science 329: 533-538.

Taylor, T. B., G. Mulley, A. H. Dills, A. S. Alsohim, L. J. McGuffin, D. J. Studholme, M. W. Silby, M. A. Brockhurst, L. J. Johnson, and R. W. Jackson. 2015. Evolutionary resurrection of flagellar motility via rewiring of the nitrogen regulation system. Science 347: 1014-1017.

Tchoufag, J., P. Ghosh, C. B. Pogue, B. Nan, and K. K. Mandadapu. 2019. Mechanisms for bacterial gliding motility on soft substrates. Proc. Natl. Acad. Sci. USA 116: 25087-25096.

Thomas, N. A., S. L. Bardy, and K. F. Jarrell. 2001. The archaeal flagellum: a different kind of prokaryotic motility structure. FEMS Microbiol. Rev. 25: 147-174.

Titus, M. A. 2016. Myosin-driven intracellular transport, Pages 265-279. In T. D. Pollard and R. D. Goldman (eds.) The Cytoskeleton. Cold Spring Harbor Laboratory Press, Cold Spring Harbor, NY.

Tocheva, E. I., E. G. Matson, D. M. Morris, F. Moussavi, J. R. Leadbetter, and G. J. Jensen. 2011. Peptidoglycan remodeling and conversion of an inner membrane into an outer membrane during sporulation. Cell 146: 799-812.

Tocheva, E. I., D. R. Ortega, and G. J. Jensen. 2016. Sporulation, bacterial cell envelopes and the origin of life. Nat. Rev. Microbiol. 14: 535-542.

Toft, C., and M. A. Fares. 2008. The evolution of the flagellar assembly pathway in endosymbiotic bacterial genomes. Mol. Biol. Evol. 25: 2069-2076.

Typas, A., M. Banzhaf, C. A. Gross, and W. Vollmer. 2011. From the regulation of peptidoglycan synthesis to bacterial growth and morphology. Nat. Rev. Microbiol. 10: 123-136.

Ursell, T. S., J. Nguyen, R. D. Monds, A. Colavin, G. Billings, N. Ouzounov, Z. Gitai, J. W. Shaevitz, and K. C. Huang. 2014. Rod-like bacterial shape is maintained by feedback between cell curvature and cytoskeletal localization. Proc. Natl. Acad. Sci. USA 111: E1025-E1034.

van Dam, T. J., M. J. Townsend, M. Turk, A. Schlessinger, A. Sali, M. C. Field, and M. A. Huynen. 2013. Evolution of modular intraflagellar transport from a coatomer-like progenitor. Proc. Natl. Acad. Sci. USA 110: 6943-6948.

Van Niftrik, L., et al. 2009. Cell division ring, a new cell division protein and vertical inheritance of a bacterial organelle in anammox planctomycetes. Mol. Microbiol. 73: 1009-1019.

Velle, K. B., and L. K. Fritz-Laylin. 2019. Diversity and evolution of actin-dependent phenotypes. Curr. Opin. Genet. Dev. 58/59: 40-48.

Veltman, D. M., and R. H. Insall. 2010. WASP family proteins: their evolution and its physiological implications. Mol. Biol. Cell 21: 2880-2893.

Veyrier, F. J., et al. 2015. Common cell shape evolution of two nasopharyngeal pathogens. PLoS Genet. 11: e1005338.

Vischer, N. O., et al. 2015. Cell age dependent concentration of *Escherichia coli* divisome proteins analyzed with ImageJ and ObjectJ. Front. Microbiol. 6: 586.

Visweswaran, G. R., B. W. Dijkstra, and J. Kok. 2011. Murein and pseudomurein cell wall binding domains of bacteria and archaea – a comparative view. Appl. Microbiol. Biotechnol. 92: 921-928.

Vollmer, W. 2011. Bacterial outer membrane evolution via sporulation? Nat. Chem. Biol. 8: 14-18.

Vollmer, W., and S. J. Seligman. 2010. Architecture of peptidoglycan: more data and more models. Trends Microbiol. 18: 59-66.

Wagstaff, J., and J. Löwe. 2018. Prokaryotic cytoskeletons: protein filaments organizing small cells. Nat. Rev. Microbiol. 16: 187-201.

Walter, W. J., and S. Diez. 2012. Molecular motors: a staggering giant. Nature 482: 44-45.

Walsby, A. E. 1994. Gas vesicles. Microbiol. Rev. 58: 94-144.

Wang, S., L. Furchtgott, K. C. Huang, and J. W. Shaevitz. 2012. Helical insertion of peptidoglycan produces chiral ordering of the bacterial cell wall. Proc. Natl. Acad. Sci. USA 109: E595-E604.

Waterbury, J. B., J. M. Willey, D. G. Franks, F. W. Valois, and S. W. Watson. 1985. A cyanobacterium capable of swimming motility. Science 230: 74-76.

Wickstead, B., and K. Gull. 2007. Dyneins across eukaryotes: a comparative genomic analysis. Traffic 8: 1708-1721.

Wickstead, B., and K. Gull. 2011. The evolution of the cytoskeleton. J. Cell Biol. 194: 513-525.

Wickstead, B., K. Gull, and T. A. Richards. 2010. Patterns of kinesin evolution reveal a complex ancestral eukaryote with a multifunctional cytoskeleton. BMC Evol. Biol. 10: 110.

Wientjes, F. B., C. L. Woldringh, and N. Nanninga. 1991. Amount of peptidoglycan in cell walls of gram-negative bacteria. J. Bacteriol. 173: 7684-7691.

Wilkes, D. E., H. E. Watson, D. R. Mitchell, and D. J. Asai. 2008. Twenty-five dyneins in *Tetrahymena:* a re-examination of the multidynein hypothesis. Cell Motil. Cytoskeleton 65: 342-351.

Wisniewski, J. R., and D. Rakus. 2014. Quantitative analysis of the *Escherichia coli* proteome. Data Brief 1: 7-11.

Wu, J. Q., and T. D. Pollard. 2005. Counting cytokinesis proteins globally and locally in fission yeast. Science 310: 310-314.

Yin, Q. Y., P. W. de Groot, L. de Jong, F. M. Klis, and C. G. De Koster. 2007. Mass spectrometric quantitation of covalently bound cell wall proteins in *Saccharomyces cerevisiae.* FEMS Yeast Res. 7: 887-896.

Young, K. D. 2006. The selective value of bacterial shape. Microbiol. Mol. Biol. Rev. 70: 660-703.

Young, K. D. 2010. Bacterial shape: two-dimensional questions and possibilities. Annu. Rev. Microbiol. 64: 223-240.

Zhang, P., W. Dai, J. Hahn, and S. P. Gilbert. 2015. *Drosophila* Ncd reveals an evolutionarily conserved powerstroke mechanism for homodimeric and heterodimeric kinesin-14s. Proc. Natl. Acad. Sci. USA 112: 6359-6364.

Zhu, S., T. Nishikino, B. Hu, S. Kojima, M. Homma, and J. Liu. 2017. Molecular architecture of the sheathed polar flagellum in *Vibrio alginolyticus.* Proc. Natl. Acad. Sci. USA 114: 10966-10971.

Figure 16.1. Examples of the structural forms involving the three key forms of fibril-forming proteins in eukaryotes. Individual tubulin filaments are comprised of heterodimers of two elemental forms of tubulin (purple and blue). Intermediate filaments can assemble into higher-order structures such as cables and sheets.

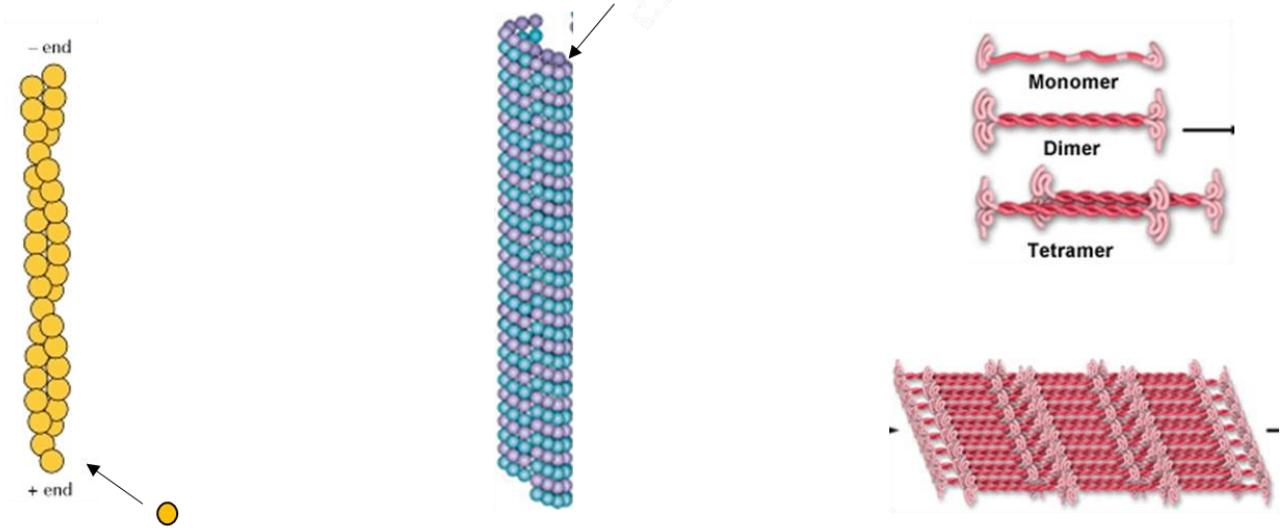

Actin Tubulin Intermediate Filaments

Figure 16.2. An example of a motor protein interfacing with a microtubule, along which it walks fueled by energy derived from ATP hydrolysis, carrying its cargo (in this case a transport vesicle).

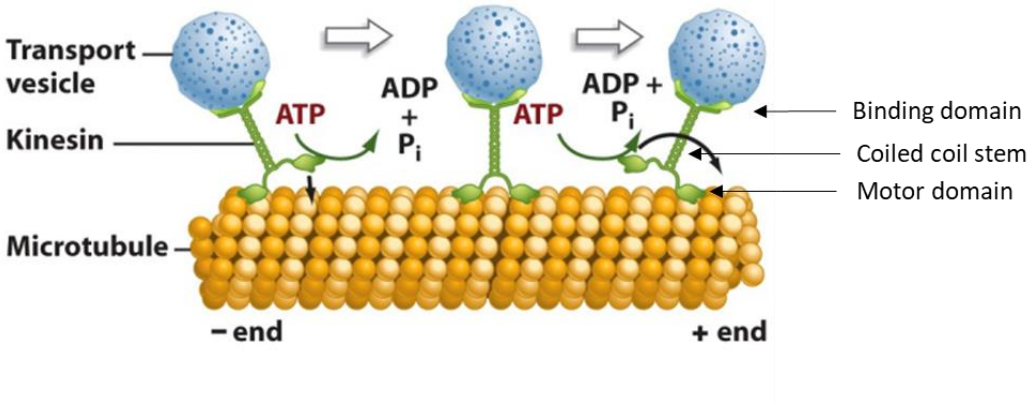

Figure 16.3. Idealized schematics of bacterial (left) and eukaryotic (right) flagella. The former emanates from a complex apparatus embedded in the double membrane. The latter grows out of a basal body (centriole), and has an interior consisting of tubulins along which motor proteins move (not shown).

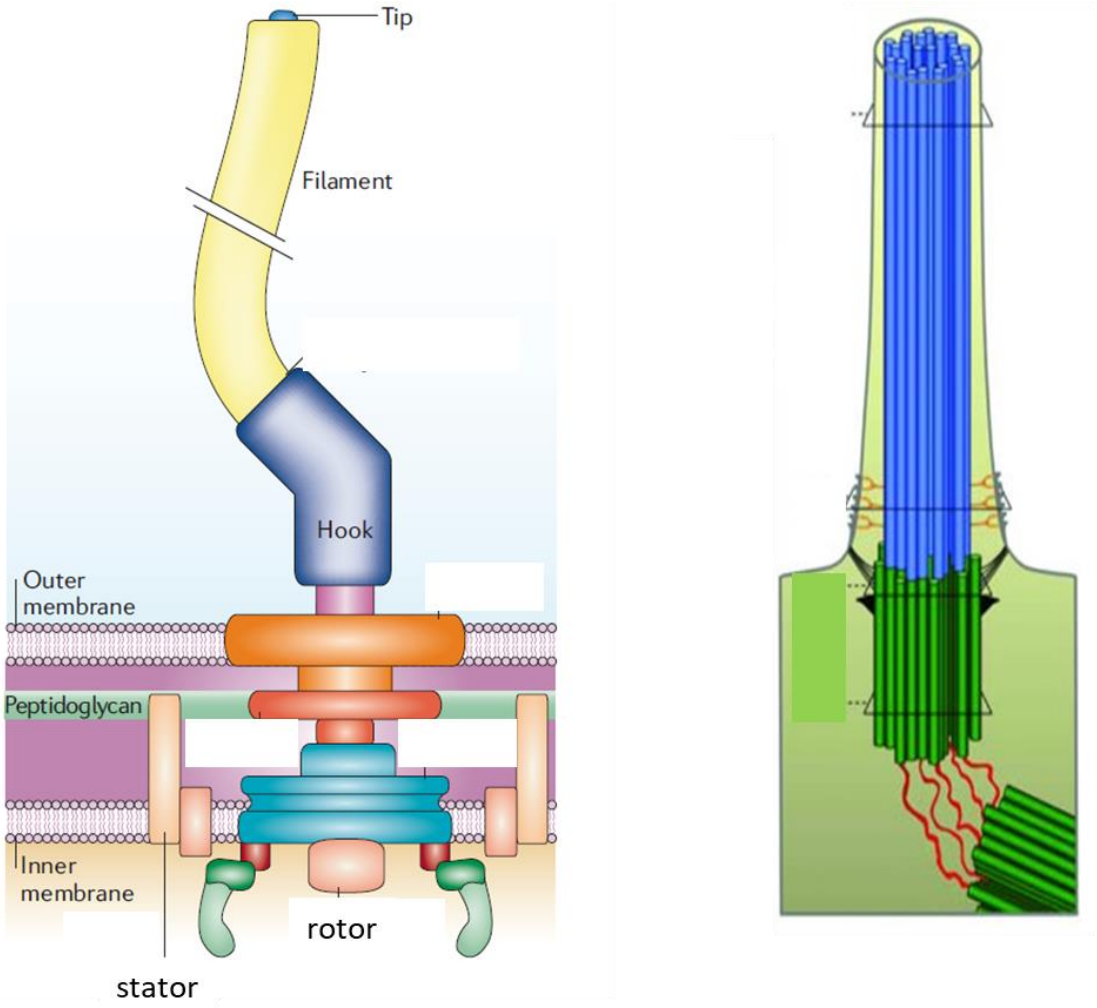

Figure 16.4. Scaling relationships between swimming velocities (v) and cell volume (V) in unicellular species. For eukaryotes, $v = 16.6V^{0.25}$, $r^2 = 0.35$); and for bacteria, $v = 29.5V^{0.17}$, $r^2 = 0.17$) (as the data are very noisy, the data for all phylogenetic groups were pooled for the eukaryote analysis). The measured values are corrected for temperature assuming a Q10 of 2.5.

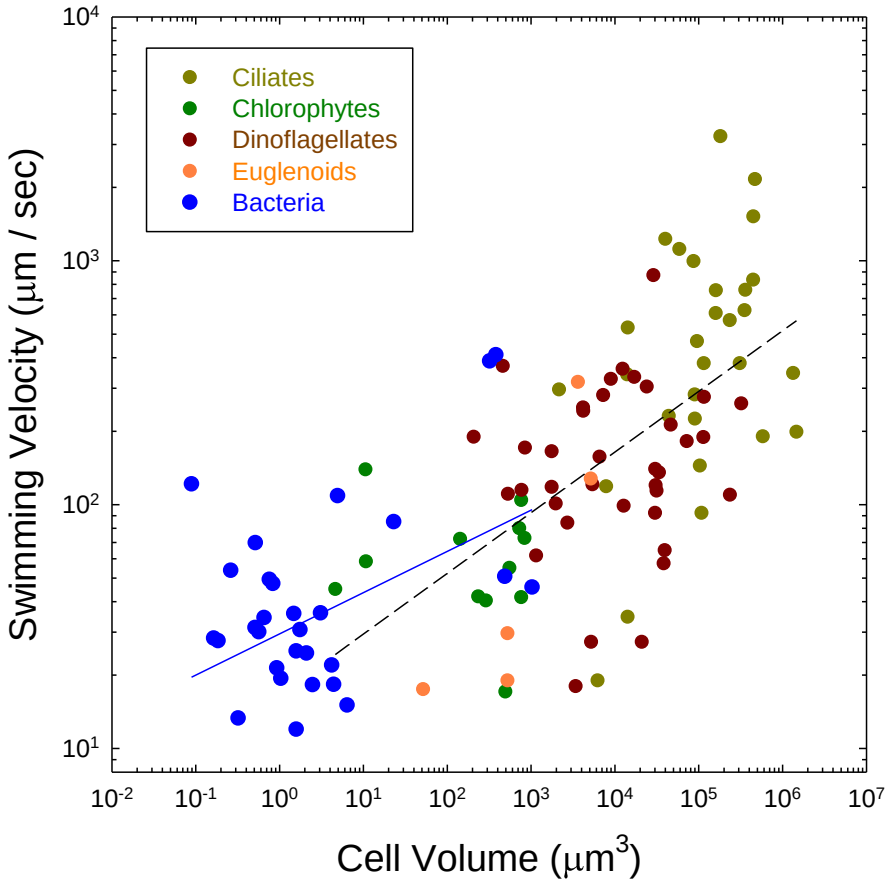

Figure 16.5. A cartoon version of a peptidoglycan layer. The paired hexagons represent dimers of NAM and NAG, whereas the small chains represent cross-linked peptides.